Anticancer ruthenium(ii) tris(pyrazolyl)methane complexes with bioactive co-ligands

(Article begins on next page)

02 May 2024

This is the final peer-reviewed accepted manuscript of:

A. Gobbo, S. Pereira, L. Biancalana, S. Zacchini, M. L. M. F. S. Saraiva, P. J. Dyson, F. Marchetti, "Anticancer Ruthenium(II) Tris(pyrazolyl)methane Complexes with Bioactive Co-ligands", *Dalton. Trans.*, **2022**, *51*, 17050-17063.

The final published version is available online at:

https://doi.org/10.1039/d2dt03009h

Anticancer Ruthenium(II) Tris(pyrazolyl)methane Complexes with Bioactive Co-ligands

Alberto Gobbo,[a] Sarah A. P. Pereira,[b] Lorenzo Biancalana,[a] Stefano Zacchini,[c] M. Lúcia M. F. S. Saraiva,[b] Paul J. Dyson,[d] Fabio Marchetti[a,*]

[a] University of Pisa, Department of Chemistry and Industrial Chemistry, Via G. Moruzzi 13, I-56124 Pisa, Italy.

[b] LAQV, REQUIMTE, Laboratório de Química Aplicada, Faculdade de Farmácia da Universidade do Porto, Portugal.

[c] University of Bologna, Department of Industrial Chemistry "Toso Montanari", Viale Risorgimento 4, I-40136 Bologna, Italy.

[d] Institut des Sciences et Ingénierie Chimiques, Ecole Polytechnique Fédérale de Lausanne (EPFL), CH 1015, Switzerland.

Corresponding Author

*E-mail address: fabio.marchetti1974@unipi.it – Webpage: https://people.unipi.it/fabio_marchetti1974/

Abstract

In comparison with Ru^{II}-arene compounds, the medicinal potential of homologous Ru^{II}-tpm compounds [tpm = tris(pyrazolyl)methane] is underexplored. Pyridine, 4-pyridinemethanol and four functionalized pyridines, synthesized from the esterification of 4-pyridinemethanol with bioactive carboxylic acids (i.e, ethacrynic acid, ibuprofen, flurbiprofen and naproxen), react with the precursor $[RuCl(\kappa^3\text{-}tpm)(PPh_3)_2]Cl$ (**1**) to afford $[RuCl(\kappa^3\text{-}tpm)(PPh_3)(L)]Cl$ (**2-7**, L = pyridine ligand), in 78-91% yields. All products were fully characterized by HR-ESI mass spectrometry, IR and multinuclear NMR spectroscopy and the solid-state structures of two of the complexes, i.e. where L = pyridine and 4-pyridinemethanol,were ascertained by single crystal X-ray diffraction.

The {Ru-tpm-PPh$_3$}assembly is stable in D_2O and in biological medium (DMEM) at 37 °C, with a tendency to slowly dissociate the pyridine ligand. The antiproliferative activity of the complexes was assessed on the cancerous A2780 and A2780cisR cell lines, and the nontumoral HEK 293T cell line, moreover inhibition assays were carried out on the complexes towards COX-2 and GSTP1 enzymes.

Keywords: bioorganometallic chemistry; metallodrugs; anticancer ruthenium complexes; trispyrazolylmethane.

Introduction

The peculiar features of transition metals, including the range of available oxidation states and coordination sites, offer to metal-based drugs an arsenal of structural diversity and modes of actions that are not accessible to organic molecules.[1,2,3] Currently, a few platinum complexes are employed in the clinical treatment against cancer, and despite their effectiveness and broad applicability, their administration is associated with severe side effects and resistance problems.[4,5,6] Therefore, efforts have been devoted to the development of alternative metal-based anticancer drugs that overcome these

drawbacks.[7] In this respect, ruthenium compounds have been intensively investigated, some even entered clinical trials, and organometallic complexes based on the [Ru^{II}(η^6-arene)] scaffold have emerged as promising candidates.[8]In particular, compounds featuring the amphiphilic 1,3,5-triaza-7-phosphaadamantane (PTA) ligand or bidentate ethylenediamine ligand, such as the lead complexes RAPTA-C[9] and RM175[10] (Figure 1A), are of current interest. The easy synthetic routes to access a wide range of related structures has stimulated the exploration of a large number of neutral and cationic ruthenium(II)-arene complexes.[11,12,13] However, in some cases, limitations arise from undesired, fast disaggregation of the complexes in aqueous media, including arene dissociation.[14,15,16,17]

The conjugation with bioactive molecules, i.e. structures playing a specific biological role, is a widely investigated and versatile strategy to modify the structure of metallodrugs, since synergy between the bioorganic fragment and the metal centre results in an enhanced potency.[18,19,20]Pyridines are found in many natural products and constitute a recurrent aromatic nitrogen heterocycle contained in FDA-approved pharmaceuticals.[21] Moreover, due to their coordination ability, pyridine and substituted pyridines have been employed as ligands for the design of many ruthenium(II) anticancer candidates,[12,22] and have found to be suitable carriers for incorporating biological groups within the Ru^{II}-arene scaffold.[23]

Tris(pyrazolyl)methane (tpm) behaves as a pseudo-arene ligand in that it can function as a six-electron donor to transition metals. However, compared to metal-arene bonding, which receives a significant contribution from π-back-donation, tpm is essentially a σ-donor,[24,25] involving tridentate coordination via three nitrogen atoms (κ^3). Switching between tri- and bidentate coordination modes may occur under some conditions, with this feature being potentially useful in catalytic applications.[26,27,28] In comparison with ruthenium(II)-arene systems, the chemistry of ruthenium(II)-tpm complexes has been much less explored, and the medicinal development of these compounds is limited. Previously, it was demonstrated that the aromatic fragment of the ruthenium(II) piano-stool frame is not essential to

provide antiproliferative activity, and alternative complexes with face-capping tri-sulphur ligands were investigated, some of them exhibiting a moderate cytotoxicity.[29,30]

To the best of our knowledge, cytotoxicity studies are restricted to a small series of complexes belonging to the families $[RuCl(\kappa^3\text{-tpm})(L)_2]PF_6$ (L = MeCN, DMSO, PMePh$_2$) and $[RuCl(\kappa^3\text{-tpm})(LL)]PF_6$ (LL= diphosphine).[31] The paucity of biological studies might be a consequence of the limited number of available synthetic pathways to add diversity to the {Ru^{II}-tpm} framework. We recently contributed to this field by disclosing a straightforward route to prepare $[RuCl(\kappa^3\text{-tpm})(PPh_3)_2]Cl$, **1**, directly from ruthenium trichloride (Figure 1B).[32] We found that **1**is an excellent starting material to obtain various derivatives upon substitution of one of the PPh$_3$ ligands, and some of these derivatives exhibited a marked antiproliferative activity against a panel of cancer cell lines, mediated in part by the inhibition of mitochondrial calcium intake.[32]

Herein, we present a general strategy to obtain pyridine adducts of **1**, also incorporating different bioactive units which have been previously conjugated with anticancer metal structures improving their biological activity. Specifically, ethacrynic acid (**EA-CO$_2$H**),[33,34,35,36] flurbiprofen (**FLU-CO$_2$H**),[36,37] ibuprofen (**IBU-CO$_2$H**)[38,39,40] and naproxen (**NAP-CO$_2$H**)[41,42] (Scheme 1). **FLU-CO$_2$H**, **IBU-CO$_2$H** and **NAP-CO$_2$H** are nonsteroidal anti-inflammatory drugs (NSAIDs), commonly used in the treatment of fever, pain or inflammation,[43,44,45]and inhibit COX enzymes. This activity is supposed to be related to anticancer effects.[46,47] On the other hand, **EA-CO$_2$H**is an inhibitor of glutathione transferase enzymes (GST), which are involved in the cellular detoxification of metal drugs.[48] **EA-CO$_2$H** was successfully incorporated in various ruthenium(II)-arene complexes,[34,35] via esterification of 4-pyridinemethanol ligand.[49] Hence, 4-pyridinemethanol was selected as a convenient bioactive carrier in the present work.
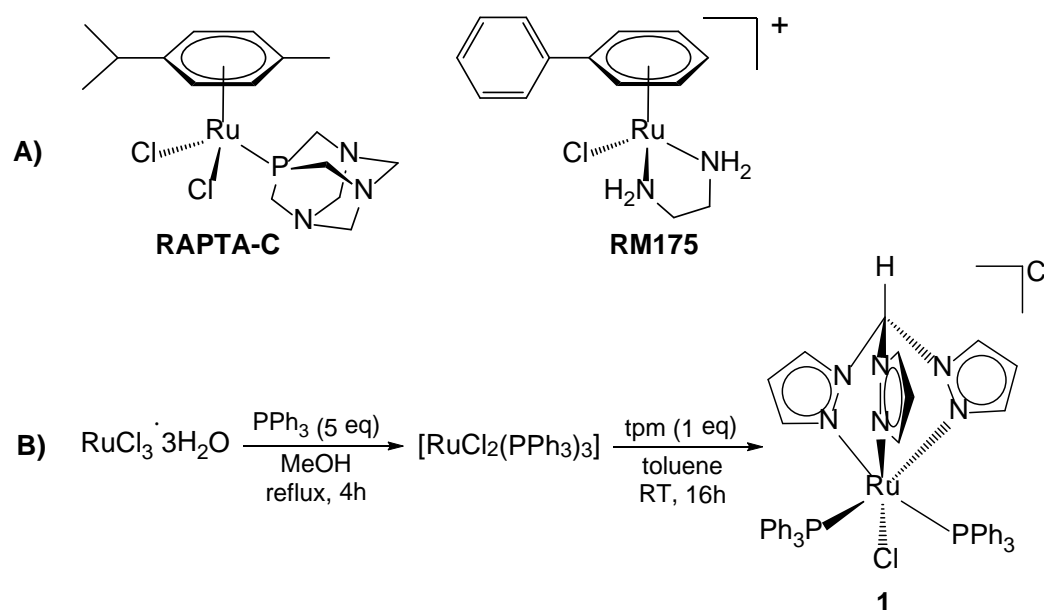
Figure 1. A) Leading ruthenium(II)-arene complexes with anticancer activity (RAPTA-C, RM175); B) Straightforward two-step procedure to access ruthenium(II)-tris(pyrazolyl)methane bis-triphenylphosphine complex (**1**).

Results and discussion

1) Synthesis and structural characterization of the ruthenium complexes

Initially, esterification of 4-pyridinemethanol with bioactive carboxylic acids was conducted in dichloromethane at room temperature using the Steglich protocol.[50] Flurbiprofen, ibuprofen and naproxen were used as racemic mixtures of enantiomers. The resulting derivatized pyridines were purified by silica chromatography and isolated in good to excellent yields (Scheme 1). The novel compounds **Py-FLU**, **Py-IBU** and **Py-NAP** were characterized by elemental analysis, IR, ^{1}H and ^{13}C NMR spectroscopy.
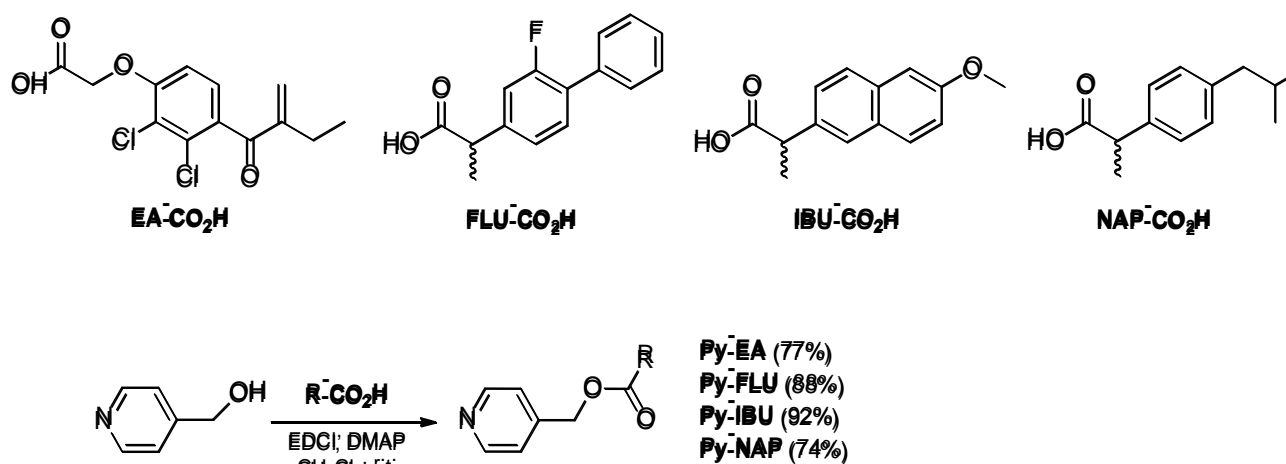
Scheme 1. Biologically active carboxylic acids investigated in this work (top, from left to right: ethacrynic acid, flurbiprofen, ibuprofen and naproxen). Bottom - general esterification reaction with 4-pyridinemethanol. **Py-EA** was previously reported,[49] while **Py-FLU**, **Py-IBU** and **Py-NAP** are unprecedented. Isolated yields in parentheses.

Next, thermal PPh$_3$-substitution reactions of **1** with pyridine, 4-pyridinemethanol and bio-functionalized pyridines were conducted in ethanol or isopropanol to afford complexes **2-7**, which were isolated in 78-91% yields by precipitation from dichloromethane (Scheme 2). The identity of **2-7** was confirmed by HR-ESI-MS analyses, showing in each case the isotopic pattern corresponding to the cation.

solvent	L	
EtOH	pyridine	**2**
EtOH	4-pyridinemethanol	**3**
^{i}PrOH	**Py-EA**	**4**
^{i}PrOH	**Py-FLU**	**5**
^{i}PrOH	**Py-IBU**	**6**
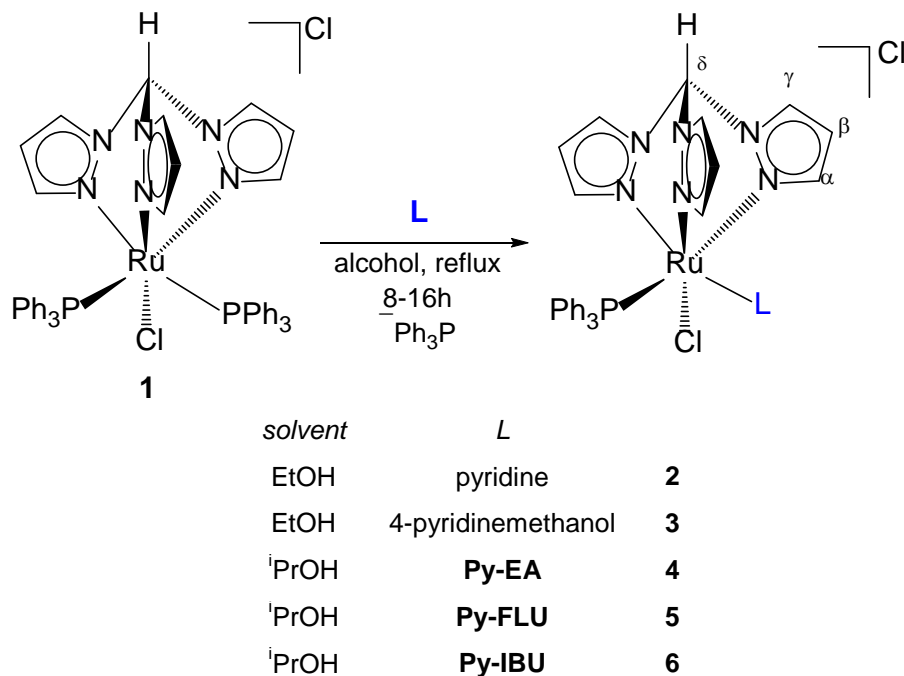
Scheme 2. Synthesis of ruthenium(II) tris(pyrazolyl)methane complexes with pyridine ligands.

The structures of **2** and **3** were elucidated by single crystal X-ray diffraction analysis (Figure 2 and Table 1). In the solid state, **2** and **3** co-crystallize with solvents, and the full formulas of the crystalline solids are **2**·CH_2Cl_2·$2H_2O$ and **3**·$3CHCl_3$. The cations of **2** and **3** closely resemble to those previously reported for related [RuCl(κ^3-tpm)(PPh$_3$)(L)]Cl compounds, with respect to the overall geometries and bonding parameters.[32] The Ru(1)-N(5) distances [2.065(4) and 2.069(3)Å in **2** and **3**, respectively], being in *trans* with respect to the pyridine ligand, are slightly shortened compared to Ru(1)-N(1) [2.094(4) and 2.120(4) Å, which are *trans* to the triphenylphosphine ligand. This data evidences the better electron-withdrawing effect of the pyridine group with respect to PPh$_3$.

Within the crystals of **2**·CH_2Cl_2·$2H_2O$, some H···Cl-type H-bonds are present that involve the co-crystallized H_2O (see Tables S1 and S2). In the case of **3**·$3CHCl_3$, H-bonds are found between the -CH_2OH groups of the aromatic ligand of the cation and the Cl$^-$ anions.

2   **3**
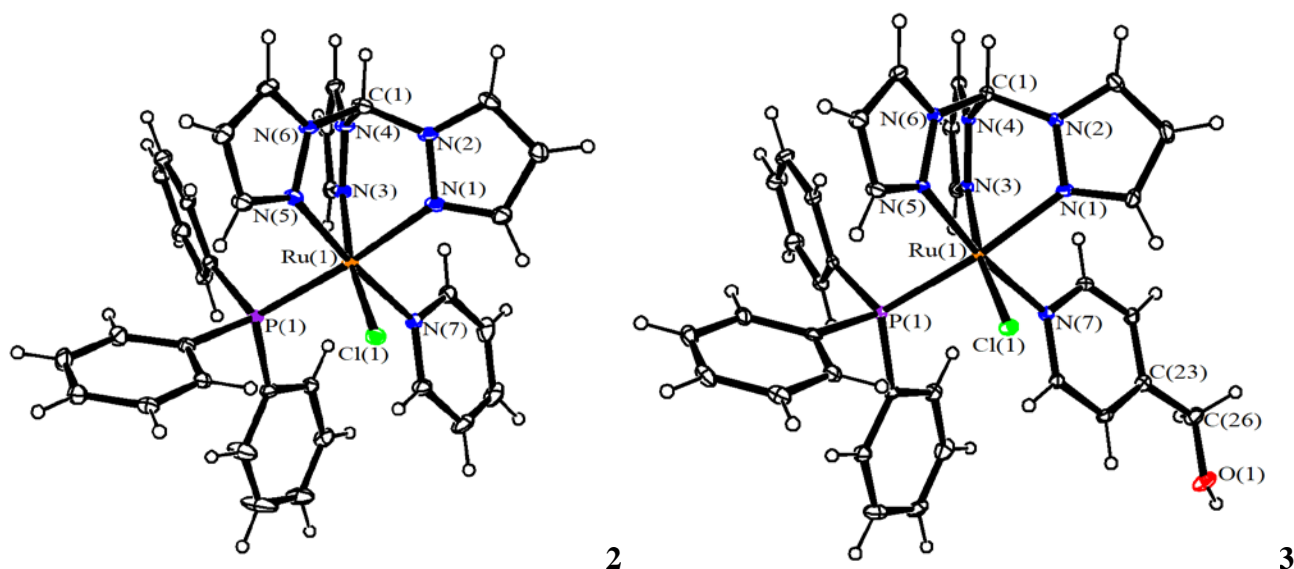
Figure 2. View of the molecular structures (ORTEP drawing) of the cations of **2** and **3**. Displacement ellipsoids are at the 30% probability level.

Table 1. Selected bond lengths (Å) and angles (°) for **2** and **3**.

	2	**3**
Ru(1)-N(1)	2.094(4)	2.120(4)
Ru(1)-N(3)	2.084(4)	2.062(3)
Ru(1)-N(5)	2.065(4)	2.069(3)
Ru(1)-P(1)	2.3312(13)	2.3241(11)
Ru(1)-Cl(1)	2.4117(12)	2.4112(10)
Ru(1)-N(7)	2.087(4)	2.096(3)
N(1)-Ru(1)-N(3)	83.48(16)	83.70(13)
N(1)-Ru(1)-N(5)	84.91(16)	83.85(13)
N(3)-Ru(1)-N(5)	87.43(16)	87.98(13)
P(1)-Ru(1)-Cl(1)	98.42(4)	97.34(4)
P(1)-Ru(1)-N(7)	93.94(12)	96.55(10)
Cl(1)-Ru(1)-N(7)	88.68(12)	88.08(10)

A salient feature in the IR spectra of **4-7** (in the solid state) is the absorption due to the ester group, occurring in the range 1736-1756 cm^{-1}, with a minor shift (within 10 cm^{-1}) from that observed for the respective functionalized pyridines. The NMR spectra of **2-4** contain single sets of resonances, while the NMR spectra of **5-7** evidence the presence of equimolar amounts of two diastereoisomers providing almost identical resonance values. In particular, the ^{31}P NMR signal is coincident for the two diastereoisomers. In general, the signals assigned to tpm are not significantly affected by the nature of the pyridine ligand, and the three pyrazolyl rings are non-equivalent, consistent with chirality at the metal atom. Upon coordination, the signals related to the pyridine {CH}protons adjacent to the nitrogen undergo an upfield shift in the ^{1}H NMR spectra and downfield in the ^{13}C NMR spectra [e.g. from 8.46 (^{1}H) and 150.4 ppm (^{13}C) to 8.02 (^{1}H) and 156.6 ppm (^{13}C), in **Py-IBU**/**6**]. The pyridine resonances do not substantially differ in the 4-pyridinemethanol complex **3** compared to the functionalized complexes **4-7**. In **4-7** the ester moiety gives rise to a ^{13}C resonance in the range 167.7-174.4 ppm, which is almost coincident to that in the free ligands. The ^{31}P NMR spectra of **2-7** show the signal related to PPh$_3$ as a singlet occurring in a restricted chemical shift interval (50.3– 51.2 ppm), that

is significantly shifted with respect to **1** (δ = 40.1 ppm).[32] The ^{19}F NMR spectrum of **5** consists of a singlet at ca. -118 ppm.

2) Solubility, partition coefficients and stability in aqueous media

The behaviour of **2-7** in aqueous media was evaluated by spectroscopic methods. Solubility in D_2O was determined by ^{1}H NMR spectroscopy using dimethyl sulfone (Me_2SO_2) as an internal standard, with the functionalized complexes **4-7** being below the detection limit of the technique (Table 2). Otherwise, **2** and **3** display appreciable water solubilities approaching that of the anticancer drug cisplatin (8.4 $mmol \cdot L^{-1}$).[51]

The octanol-water partition coefficients (Log P_{ow}, Table 2) of **2-7** were measured by a UV-Vis method;[52] Log P_{ow} values were obtained after ca. 20 minutes from the dissolution of the complexes, and evidence an amphiphilic (or moderately hydrophilic) character for **2-4**. The other bio-functionalized complexes **5-7** are substantially lipophilic.

Table 2. Solubility in water (D_2O, 21° C, ^{1}H NMR, Me_2SO_2 as internal standard) and octanol/water partition coefficient (Log P_{ow}, UV-Vis)of ruthenium complexes.

Compound	Solubility/ 10^{-3} $mol \cdot L^{-1}$ [a]	Log P_{ow}
2	2.3	-0.04 ± 0.05
3	3.3	-0.25 ± 0.04
4	< $1 \cdot 10^{-4}$	0.46 ± 0.02
5	< $1 \cdot 10^{-4}$	> 2
6	< $1 \cdot 10^{-4}$	> 2
7	< $1 \cdot 10^{-4}$	> 2

Next, the speciation of **2-7**in aqueous solutions was investigated by ^{1}H and ^{31}P NMR spectroscopy at 37 °C. On a timescale considerably longer than that required for the Log P_{ow} quantitation, **2** and **3** in D_2O (and D_2O/CD_3OD mixture) undergo an equilibrium process consisting of chloride-water exchange, affording the respective bis-cationic aquo-species **2**^{W} and **3**^{W} (Scheme 3A). The same

behaviour was previously recognized for related complexes with different monodentate ligands.[32] NMR data of 2^W and 3^W are reported in the Supporting Information (Figures S40-S47 and Table S3). The aquo-complexes were detected in a variable relative amount after 3 hours (2^W, 13%; 3^W, 42%), and became the largely prevalent species in solution after 48hours, when the system had probably reached equilibrium.

A parallel experiment on **3** revealed a significant increase of the molar conductivity of a 10^{-3} M H_2O solution during 24 hours (from 133 to 206 $S \cdot cm^2 \cdot mol^{-1}$),reflecting the increase by one unit of the net cationic charge of the complex. Moreover, 3^W (isolated from the D_2O solution) slowly reverts to **3** once dissolved in neat CD_3OD, thus indicating that the chloride/water substitution is reversible (Figures S44-S45). The chloride-water exchange recognized for **2-3** resembles the behaviour of RAPTA complexes, for which the dissociation of one/two chloride ligand(s) in physiological environment is considered a key to the activation of the drug.[9,53,54,55] Note that this process occurs on a significantly longer time-scale for the Ru^{II}-tpm complexes compared to Ru^{II}-arene compounds.[53,54,55]

Since **4-7** are almost insoluble in water, dimethylsulfoxide was used to assist dissolution during cytotoxicity tests, and hence the behaviour of these complexes was studied in DMSO-d_6/D_2O mixtures. For comparison, complexes **2** and **3** were also tested under the same conditions (Figures S48-S54 and Table S4). Despite the presence of water, displacement of chloride was not observed by NMR spectroscopy in every case, where as slow, partial displacement of the pyridine ligand was detected (formation of **8**, Scheme 3B). NMR spectra of **6**dissolved in neat DMSO-$d_6$match spectra in DMSO-d_6/D_2O,[56] thus **8** was attributed to a DMSO adduct. Attempts to synthesize and isolate **8** were unsuccessful, e.g. the reaction of **1** with DMSO (20eq.) in boiling EtOH gave **8** in only modest yield after 16 hours. The yield increased to 74% by using a larger excess of DMSO (50eq.), but in this case a secondary product formed in appreciable amounts (ca.18% based on ^{1}H NMR spectroscopy).
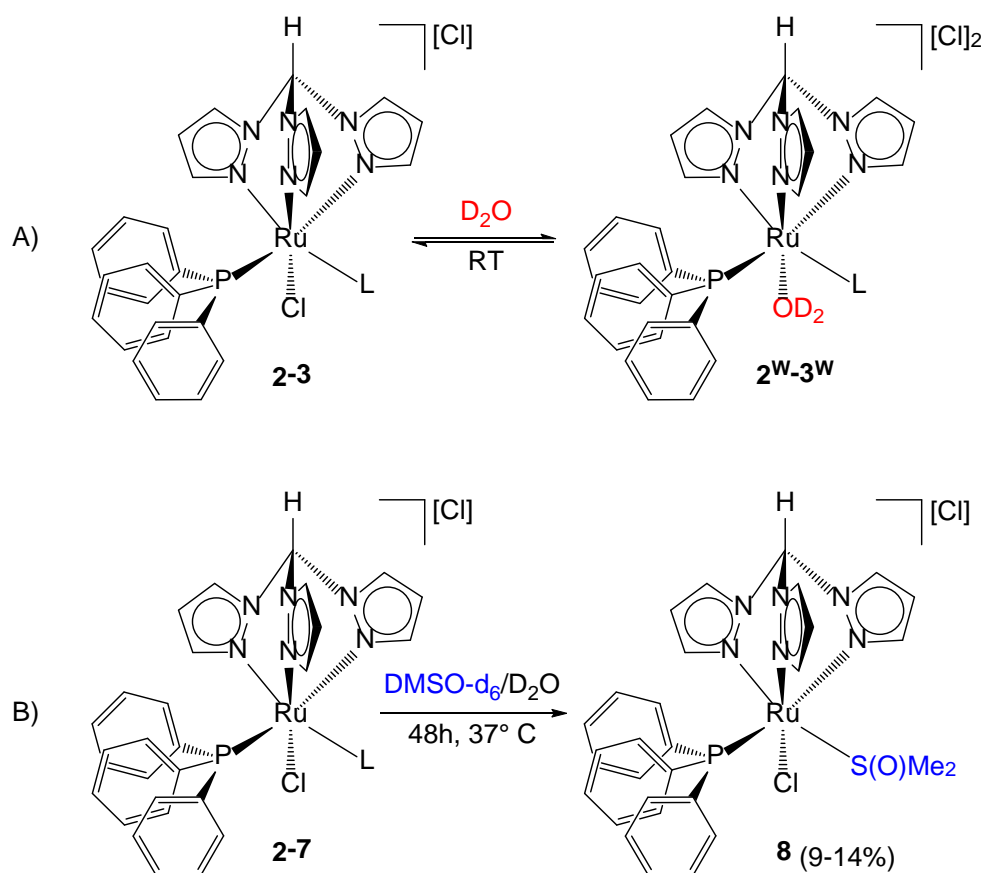
Scheme 3. Speciation of Ru^{II}-tpm complexes in aqueous solutions. A) Reversible chloride dissociation from water soluble complexes in D$_2$O. B) Dissociation of functionalized pyridine ligands in DMSO-d$_6$/D$_2$O.

The behaviour of **2-7** was also analysed in deuterated cell culture medium(DMEM-d), at 37 °C. The presence of *ca*. 0.1 M chloride ion in the medium retards and disfavours chloride dissociation from **2-3** (Tables S3-S4). To achieve an appreciable solubility in DMEM-d, complexes **4-7** required a large co-volume of DMSO-d$_6$, anyway the conversion of **4-7** into **8** remains low (< 15%) after 24 hours (Table S4).

ESI-MS analysis of a diluted solution of **3** in H$_2$O, performed at different times after the dissolution, confirmed the occurrence of ready chloride dissociation (m/z = 343.5729, corresponding to [Ru(tpm)(PPh$_3$)(Py)]$^{2+}$ which is suggestive of the formation in solution of the water adduct [Ru(tpm)(PPh$_3$)(Py)(OH$_2$)]$^{2+}$), and evidenced a tendency for slow pyridine release (m/z = 613.0626,

corresponding to $[RuCl(tpm)(PPh_3)]^+$ suggestive of the formation of $[RuCl(tpm)(PPh_3)(OH_2)]^+$), see Figure S55.

According to NMR experiments on CD_3OD/D_2O solutions, fast alcoholysis releasing ethacrynic acid occurred from **4**, whereas **5-7** proved to be generally more robust even after 24 hours.[57] Note that it was previously hypothesized that intracellular esterases are implicated in separating $EA-CO_2H$ from the ligand/complex block.[58,59,60]

Overall, stability studies in several aqueous media highlight the robustness of the Ru^{II}-tpm-PPh_3 scaffold and suggest that the release in the physiological environment of the bioactive payload, prevalently in the form of pyridine-methanol ester, may slowly take place from **4-7**. Nevertheless, pyridine dissociation occurs more slowly than analogous ruthenium(II)-arene complexes of the type $[RuCl_2(\eta^6\text{-}p\text{-cymene})(\text{pyridine})]$ (approximately, 35% after 17 h and 75% after 72 h, in $D_2O/DMSO\text{-}d_6$ mixtures).[49]

3) Biological studies

The antiproliferative activity of **2-7** and of the related bioactive carboxylic acids was assessed on A2780 and A2780cisR cancer cell lines and the nontumoral HEK293T cell line (Table 3). Cisplatin and RAPTA-C were used as positive and negative controls, respectively. The complexes are cytotoxic towards all the cell lines including the HEK 293T cell line, highlighting the absence of cancer cell selectivity. In general, IC_{50} values are in alignment with Log P_{ow} coefficients, suggesting that the lipophilicity of the compounds is rather influencing on the antiproliferative activity.

Table 3. IC_{50} values (µM) determined for **2-7**, cisplatin, RAPTA-C and bioactive carboxylic acids on human ovarian carcinoma (A2780), human ovarian carcinoma cisplatin resistant (A2780cisR) and human embryonic kidney (HEK 293T) cell lines after 72 h exposure. Values are given as the mean ± SD.

	A2780	A2780cisR	HEK 293T
2	8 ± 3	15 ± 9	10 ± 4

Compound	C$_{50}$ ± SD (μM), COX-2	IC$_{50}$ ± SD (μM), GST-P1
3	26 ± 10	26 ± 5	47 ± 8
4	12 ± 2	20 ± 5	10 ± 3
5	4.5 ± 0.6	8 ± 2	4 ± 2
6	5 ± 1	10 ± 2	4.3 ± 0.8
7	6 ± 1	14 ± 4	5 ± 1
Ethacrynic acid	38 ± 2	38 ± 10	27 ± 11
Flurbiprofen	> 100	> 100	> 100
Ibuprofen	> 100	> 100	85 ± 6
Naproxen	> 100	> 100	100 ± 2
Cisplatin	0.5 ± 0.1	3.3 ± 0.5	1.4 ± 0.9
RAPTA-C	99 ± 3	> 200	> 200

COX-2 inhibition assays were performed on the bio-functionalized ruthenium compounds **4-7**, the non-functionalized one **3** and related bioactive molecules (Table 4). Complexes **3**, **5**, **6** and **7** inhibit COX-2 enzyme, and a slightly higher activity was obtained with **6** and **7**, containing ibuprofen and naproxen, compared to **3**. In general, the ruthenium complexes display a stronger inhibitory activity towards COX-2 with respect to flurbiprofen, ibuprofen and naproxen, in alignment with previous studies showing the effective inhibiting capacity of a series of organo-ruthenium and platinum complexes.[61,62]

Complexes **3** and **4** were additionally investigated for their capability of inhibiting GSTP1, and evidenced a poor activity compared to ethacrynic acid, although being slightly higher for the ethacrynic acid complex **4**. This outcome points out that the incorporation of EA-CO$_2$H within the structure of **4** is ineffective, and the modest GSTP1 inhibition exerted by this compound is imputable to minor release of the pyridine ligand and/or ethacrynic acid (see above).

Table 4. IC$_{50}$ values (μM) obtained for ruthenium complexes and bioactive carboxylic acids in the inhibition of COX-2 and GSTP1 enzymes.

3	81 ± 4	216 ± 10
4		126 ± 4
5	74 ± 6	
6	59 ± 4	
7	43 ± 1	
Ethacrynic acid		13.58 ± 0.02[62]
Flurbiprofen	719 ± 135 [62]	
Ibuprofen	> 3000	
Naproxen	> 3000	

Conclusions

Ruthenium(II) tris(pyrazolyl)methane complexes constitute an intriguing class of coordination compounds, for which biological studies are rare in the literature. Here, we describe a straightforward synthetic strategy to tether bioactive molecules to the metal scaffold by means of a pyridine carrier, and stability studies highlight the substantial robustness of the complexes in aqueous solutions. The cytotoxicity profiles are similar for functionalized and non-functionalized complexes and, in combination with COX-2 and GSTP1 enzyme inhibition assays, indicate that the antiproliferative activity is not closely linked to the inhibition of these enzymes. It is possible that the presence of bulky tpm and PPh$_3$ groups, which are firmly bound to the ruthenium centre, reduces the possibility of interaction with the enzymes, although further studies would be needed to confirm this hypothesis.

Experimental

1. General remarks. Reactants and solvents were purchased from Alfa Aesar, Merck, Strem or TCI Chemicals, and were of the highest purity available. Complex **1**[32] and tris(1-pyrazolyl)methane (tpm)[63] were prepared according to literature methods. Reactions were conducted under a N$_2$ atmosphere using

standard Schlenk techniques, and all isolated products were stored in air. Solvents were used as received unless otherwise stated. Toluene and diethyl ether were dried with the solvent purification system mBraun MB SPS5, while methanol was distilled from calcium hydride and isopropanol from magnesium. IR spectra of solid samples were recorded on Agilent Cary630 FTIR spectrometer, then IR spectra were processed with Spectragryph software.[64] NMR spectra were recorded at 298 K on a Jeol JNM-ECZ500R instrument equipped with a Royal HFX Broadband probe. Chemical shifts (expressed in parts per million) are referenced to the residual solvent peaks (^{1}H, ^{13}C)[65] or to external standard (^{19}F to CFCl$_3$, ^{31}P to H$_3$PO$_4$). ^{1}H and ^{13}C{^{1}H}NMR spectra were assigned with the assistance of ^{1}H-^{13}C (gs-HSQC and gs-HMBC) correlation experiments.[66] Elemental analyses were performed on a Vario MICRO cube instrument (Elementar).Conductivity measurements were carried using an XS COND 8 instrument (cell constant = 1.0 cm^{-1}) equipped with NT 55 temperature probe (measurements automatically adjusted to 25 °C). Mass spectrometry experiments were conducted with Waters XEVO G2-S QTOF; the technique used was electrospray ionization (ESI) and the analyser quadrupole time-of-flight mass spectrometry (QTOF MS) with positive ion mode (ES+) and a full width at half maximum of 0.01 by direct injection of the samples.

General procedure for the synthesis of pyridines

A solution of 4-pyridinemethanol and the appropriate carboxylic acid, in anhydrous dichloromethane (15 mL), was treated with EDCI·HCl and DMAP. The resulting mixture was allowed to stir at room temperature for 16h. Then the volatiles were evaporated under reduced pressure and the crude product purified by silica chromatography.

**Pyridin-4-yl-methyl-2-(2,3-dichloro-4-(2-methylenebutanoyl)phenoxy)acetate, Py-EA(Chart 1)[49]**

Chart 1. Structure of **Py-EA**(labelling refers to carbon atoms).
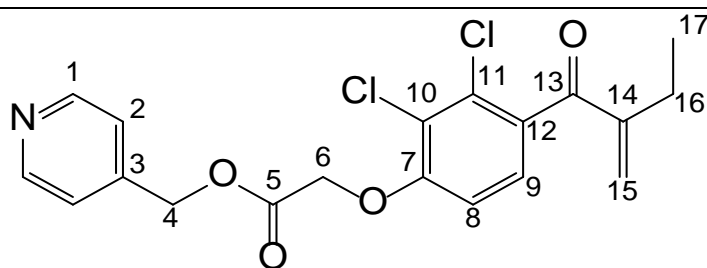
From 4-pyridinemethanol (140.0 mg, 1.28 mmol), ethacrynic acid (427 mg, 1.41 mmol), EDCI·HCl (294 mg, 1.54 mmol) and DMAP (30 mg, 0.26 mmol). Chromatography: hexane/Et$_2$O (from 2:1 v/v to 1:2 ratio). Colourless solid stored at −30 °C, yield 304 mg (77%). Anal. calcd. for C$_{19}$H$_{17}$Cl$_2$NO$_4$: C, 57.88; H, 4.35; N, 3.55. Found: C, 57.75; H, 4.40; N, 3.62. IR (solid state): $\tilde{\nu}$/cm^{-1} = 3031w, 2988m, 2966m, 2902m, 2877m, 1758s ($\tilde{\nu}_{C=O}$), 1666s, 1604m, 1583m, 1560m, 1470m, 1443m, 1414m, 1392m, 1381m, 1365m, 1324w, 1288m, 1262m, 1246m, 1200s, 1174m, 1123m, 1077s, 1067s, 1003m, 990m, 943m, 891m, 844w, 825m, 806s, 765m, 728m, 634m, 567m, 475m. ^{1}H NMR (CDCl$_3$): δ/ppm = 8.61 (d, 2H, $^3J_{HH}$ = 6.0 Hz, C^{1}H); 7.23 (d, 2H, $^3J_{HH}$ = 5.9 Hz, C^{2}H); 7.10 (d, 1H, $^3J_{HH}$ = 8.4 Hz, C^{9}H); 6.76 (d, 1H, $^3J_{HH}$ = 8.5 Hz, C^{8}H); 5.94, 5.58 (s, 2H, C^{15}H); 5.26 (s, 2H, C^{4}H); 4.85 (s, 2H, C^{6}H); 2.45 (q, 2H, $^3J_{HH}$ = 7.4 Hz, C^{16}H); 1.15 (t, 3H, $^3J_{HH}$ = 7.3 Hz, C^{17}H).

Pyridin-4-yl-methyl 2-(2-fluoro-[1,1'-biphenyl]-4-yl)propanoate, Py-FLU (Chart 2)

Chart 2. Structure of **Py-FLU**(labelling refers to carbon atoms).
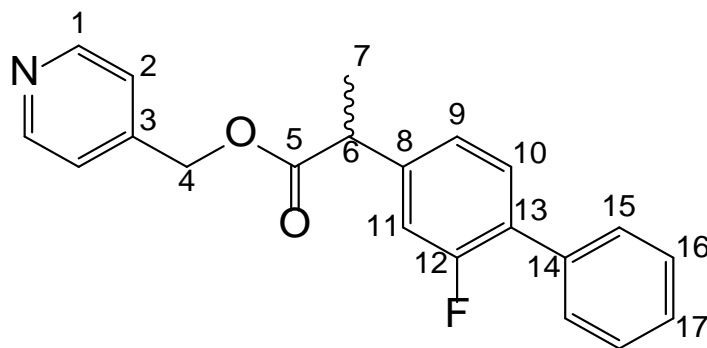
From 4-pyridinemethanol (140 mg, 1.28 mmol), flurbiprofen (racemic mixture; 344 mg, 1.41 mmol), EDCI·HCl (294 mg, 1.54 mmol) and DMAP (30 mg, 0.26 mmol). Chromatography: petroleum ether/Et$_2$O (from 2:1 v/v to 1:2 ratio). Colourless solid stored at −30 °C, yield 295 mg (88%). Anal. calcd for. C$_{21}$H$_{18}$FNO$_2$: C, 75.21; H, 5.41; N, 4.18. Found: C, 74.95; H, 5.50; N, 4.16. IR (solid state): $\tilde{v}$/cm^{-1} = 3070w, 3031w, 2978w, 2911w, 1727s ($\tilde{v}_{C=O}$), 1623w, 1601m, 1581w, 1563m, 1482m, 1460m, 1449w, 1415m, 1382w, 1372w, 1328w, 1319w, 1309w, 1243w, 1221m, 1186s, 1151m, 1131m, 1095m, 1068m, 1026m, 1009m, 990w, 978w, 923m, 871m, 840m, 826m, 801s, 760s, 735w, 725w, 691s, 636m, 579m, 526w, 474m. ^{1}H NMR (CD$_2$Cl$_2$): δ/ppm = 8.52 (d, 2H, $^3J_{HH}$ = 5.2 Hz, C^{1}H); 7.56-7.53 (m, 2H, C^{15}H); 7.45-7.37 (m, 4H, C^{16}H + C^{10}H + C^{17}H); 7.17 (dd, 1H, $^3J_{HH}$ = 7.9 Hz, $^4J_{HH}$ = 1.9 Hz, C^{9}H); 7.16-7.13 (m, 1H, C^{11}H); 7.14 (m, 2H, C^{2}H); 5.14 (s, 2H, C^{4}H); 3.88 (q, 1H, $^3J_{HH}$ = 7.1 Hz, C^{6}H); 1.57 (d, 3H, $^3J_{HH}$ = 7.1 Hz, C^{7}H). ^{13}C{^{1}H} NMR (CD$_2$Cl$_2$): δ/ppm = 173.9 (C^5); 160.1 (d, C^{12}, $^1J_{CF}$ = 247.9 Hz); 150.4 (C^1); 145.3 (C^3); 142.1 (d, $^3J_{CF}$ = 7.8 Hz, C^8); 135.8 (d, $^3J_{CF}$ = 1.1 Hz, C^{14}); 131.3 (d, $^3J_{CF}$ = 3.7 Hz, C^{10}); 129.3 (d, $^3J_{CF}$ = 3.0 Hz, C^{15}); 128.9 (C^{16}); 128.3 (d, $^2J_{CF}$ = 13.6 Hz, C^{13}); 128.2 (C^{17}); 124.1 (d, $^4J_{CF}$ = 3.4 Hz, C^9); 122.0 (C^2); 115.7 (d, $^2J_{CF}$ = 23.6 Hz, C^{11}); 65.0 (C^4); 45.5 (d, $^4J_{CF}$ = 1.3 Hz, C^6); 18.6 (C^7). ^{19}F NMR (CD$_2$Cl$_2$): δ ppm = -118.3.

Pyridin-4-yl-methyl 2-(4-isobutylphenyl)acetate, Py-IBU (Chart 3)

Chart 3. Structure of **Py-IBU** (labelling refers to carbon atoms).
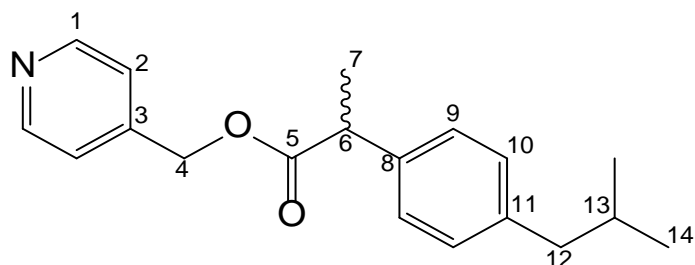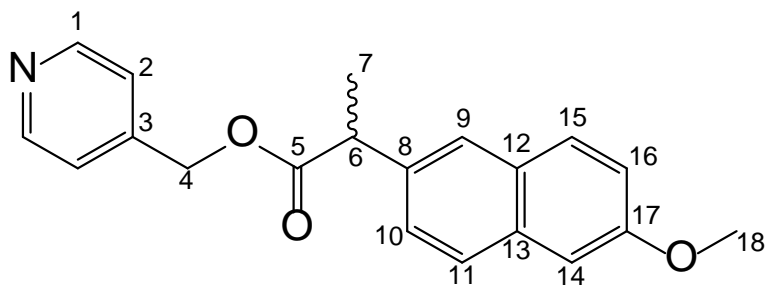

From 4-pyridinemethanol (140 mg, 1.28 mmol), ibuprofen (racemic mixture; 290 mg, 1.41 mmol), EDCI·HCl (294 mg, 1.54 mmol) and DMAP (30 mg, 0.26 mmol). Chromatography: hexane/Et$_2$O (from

2:1 v/v to 1:2 ratio). Colourless oil stored at −30 °C, yield 334 mg (92%).Anal. calcd. for $C_{19}H_{23}NO_2$:

C, 76.73; H, 7.80; N, 4.71. Found: C, 76.95; H, 7.74; N, 4.63. IR (solid state): $\tilde{\upsilon}/cm^{-1}$ = 3024w, 2988m,

2951m, 2929m, 2871w, 1735s ($\tilde{\upsilon}_{C=O}$), 1603m, 1562w, 1512w, 1454w, 1414m, 1378w, 1333w, 1318w,

1223w, 1198w, 1157s, 1091m, 1068m, 1020w, 992w, 848w, 793m, 724w, 582w, 550w, 472w. ^{1}H

NMR (CD_2Cl_2): δ/ppm = 8.46 (d, 2H, $^3J_{HH}$ = 6.1 Hz, C^1H); 7.22-7.11 (m, 4H, C^9H + C^{10}H); 7.05 (d,

2H, $^3J_{HH}$ = 5.6 Hz, C^2H); 5.12 (AB system, $^1J_{HH}$ = 14.0 Hz, 2H, C^4H); 3.80 (q, 1H, $^3J_{HH}$ = 7.2 Hz,

C^6H); 2.46 (d, 2H, $^3J_{HH}$ = 7.2 Hz, C^{12}H); 1.89 (hept, $^3J_{HH}$ = 6.8 Hz 1H, C^{13}H); 1.50 (d, 3H, $^3J_{HH}$ = 7.2

Hz, C^7H); 0.90 (d, 6H, $^3J_{HH}$ = 6.6 Hz, C^{14}H). $^{13}C\{^1H\}$ NMR (CD_2Cl_2): δ/ppm = 174.6 (C^5); 150.4 (C^1);

145.7 (C^3); 141.3 (C^{11}); 138.0 (C^8); 129.9 (C^9); 127.7 (C^{10}); 121.8 (C^2); 64.6 (C^4); 45.5 (C^{12}); 45.4 (C^6);

30.7 (C^{13}); 22.6 (C^{14}); 18.6 (C^7).

Synthesis of pyridin-4-yl-methyl 2-(6-methoxynaphthalen-2-yl)propanoate, Py-NAP (Chart 4)

Chart 4. Structure of **Py-NAP**(labelling refers to carbon atoms).

From 4-pyridinemethanol (140 mg, 1.28 mmol), naproxen (racemic mixture; 325 mg, 1.41 mmol),

EDCI·HCl (294 mg, 1.54 mmol) and DMAP (30 mg, 0.26 mmol). Chromatography: hexane/Et$_2$O (from

2:1 v/v to 1:2 ratio). The obtained solid was further purified by diethyl ether/H$_2$O extraction. Colourless

oil stored at −30 °C, yield 320 mg (74%). Anal. calcd. for $C_{20}H_{19}NO_3$: C, 76.73; H, 7.80; N, 4.71.

Found: C, 76.61; H, 7.91; N, 4.61. IR (solid state): $\tilde{\upsilon}/cm^{-1}$ = 3067w, 3037w, 2978m, 2957m, 2920m,

2956w, 1728s ($\tilde{\upsilon}_{C=O}$), 1622w, 1602m, 1581w, 1563m, 1483m, 1458m, 1448w, 1414s, 1381w, 1372w,

1327w, 1317w, 1309m, 1242m, 1219m, 1183s, 1151m, 1131m, 1094m, 1067m, 1027m, 1008m, 990w, 979w, 923m, 971m, 839m, 825m, 801s, 786m, 760s, 735m, 724m, 692s, 636m, 578s, 526m, 472s, 443m, 410m. ^{1}H NMR (CD$_2$Cl$_2$): δ/ppm = 8.46 (d, 2H, $^3J_{HH}$ = 5.0 Hz, C^{1}H); 7.72 (d, 2H, $^3J_{HH}$ = 7.3 Hz, C^{11}H + C^{15}H); 7.68 (s, 1H, C^{14}H); 7.41 (d, 1H, $^3J_{HH}$ = 8.5 Hz, C^{16}H); 7.2 (s, 1H, C^{9}H); 7.15 (d, 1H, $^3J_{HH}$ = 7.6 Hz, C^{10}H); 7.08 (d, 2H, $^3J_{HH}$ = 5.1 Hz, C^{2}H); 5.15 (m, 2H, C^{4}H); 3.97 (q, 1H, $^3J_{HH}$ = 7.2 Hz, C^{6}H); 3.91 (s, 3H, C^{18}H); 1.60 (d, 3H, $^3J_{HH}$ = 7.1 Hz, C^{7}H). ^{13}C{^{1}H} NMR (CD$_2$Cl$_2$): δ/ppm = 174.6 (C^5); 158.4 (C^{17}); 150.4 (C^1); 145.6 (C^3); 135.9 (C^8); 134.4 (C^{13}); 129.7 (C^{15}); 129.5 (C^{14}); 127.7 (C^{11}); 126.8 (C^9); 126.6 (C^{10}); 122.0 (C^2); 119.6 (C^{16}); 106.2 (C^{14}); 67.9 (C^4); 55.8 (C^{18}); 45.9 (C^6); 18.7 (C^7).

General procedure for the synthesis of complexes [RuCl(κ^3-tpm)(PPh$_3$)(L)]Cl.

A solution of **1** and the appropriate ligand L, in either ethanol or anhydrous isopropanol, was heated at reflux for a variable time. After cooling to room temperature, the volatiles were evaporated under reduced pressure. The crude product was purified by reprecipitation from dichloromethane and finally dried under vacuum.

## [RuCl(κ^3-tpm)(PPh$_3$)(pyridine)]Cl, 2 (Chart 5)

Chart 5. Structure of **2**(labelling refers to carbon atoms).
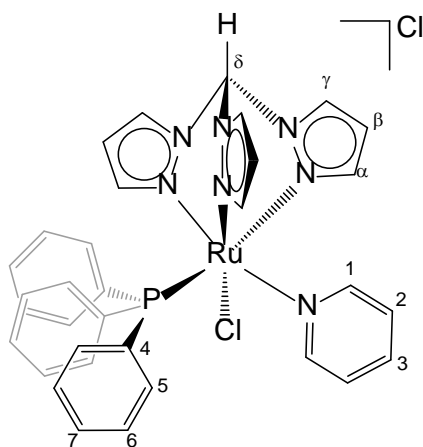
From **1** (200 mg, 0.22 mmol) and pyridine (24.8 µL, 0.31 mmol) in ethanol (10 mL). Reaction time 16

h. Yellow solid, yield 145 mg (91%). Anal. calcd. for $C_{33}H_{30}Cl_2N_7PRu$: C, 54.47; H, 4.16; N, 13.48;

Cl, 9.75. Found: C, 54.36; H, 4.22; N, 13.41; Cl, 9.68. HR-ESI-MS (methanol): $[M]^+$ m/z = 692.1042

(theoretical for $[C_{33}H_{30}ClN_7PRu]^+$: m/z = 692.1065.IR (solid state): $\tilde{\upsilon}/cm^{-1}$ = 3109w, 3074w, 2972w,

2868w, 2757w, 2723w, 2678w, 2612w, 2589w, 2563w, 1482m, 1446m, 1432m, 1412m, 1290m,

1254m, 1220m, 1087m, 1061m, 1046m, 989w, 854m, 790m, 777m, 754s, 695s, 609m, 528s, 512m,

501m, 448m, 423m. ^{1}H NMR (CDCl$_3$): δ/ppm = 12.44 (s, 1H, C$^\delta$H); 9.08, 8.80, 8.76 (d, 3H, $^3J_{HH}$ = 3.1

Hz, C$^\gamma$H); 8.12 (s-br, 2H, C^{1}H); 7.58 (t, 1H, $^3J_{HH}$ = 7.6 Hz, C^{3}H); 7.34 (m, 3H, C^{7}H); 7.33, 7.08, 6.61

(d, 3H, C$^\alpha$H); 7.17 (t-br, 6H, C^{6}H); 6.97 (t-br, 6H, C^{5}H); 6.91 (t, 2H, $^3J_{HH}$ = 6.5 Hz, C^{2}H); 6.33, 6.12,

6.03 (t-br, 3H, $^3J_{HH}$ = 2.6 Hz C$^\beta$H). ^{13}C{^{1}H} NMR (CDCl$_3$): δ/ppm = 156.6 (C^1); 148.9, 148.2, 144.4

(C$_\alpha$); 136.1, 135.1, 133.8 (C$_\gamma$); 135.6 (C^3); 133.9 (d, $^3J_{CP}$ = 9.3 Hz, C^7); 132.0 (d, $^1J_{CP}$ = 40.8 Hz, C^5);

130.1 (C^8); 128.4 (d, $^2J_{CP}$ = 9.1 Hz, C^6); 124.0 (C^2); 108.6, 108.5, 108.4 (C$^\beta$); 74.4 (C$^\delta$). ^{31}P{^{1}H} NMR

(CDCl$_3$): δ/ppm = 51.2.ESI$^+$-MS: m/z (MeOH) = 692.10 ([M]$^+$); 577.08 ([M-Py-Cl-H]$^+$); 613.06 ([M-

Py]$^+$). Crystals suitable for X-ray diffraction were collected by slow evaporation of a CDCl$_3$ solution of

2.

[RuCl(κ^3-tpm)(PPh$_3$){N(CH)$_4$C(CH$_2$OH)}]Cl, 3 (Chart 6)

Chart 6. Structure of **3**(labelling refers to carbon atoms).
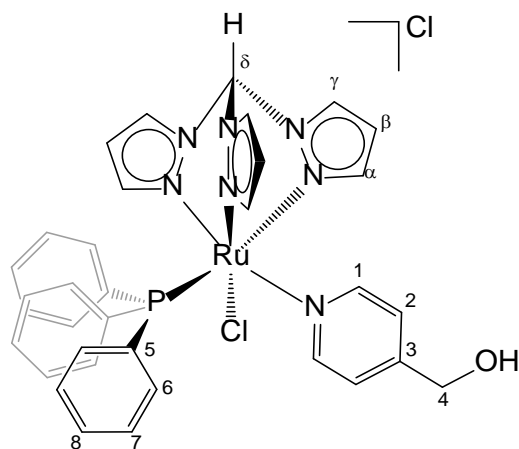
From **1** (150 mg, 0.16 mmol) and 4-pyridinemethanol (27 mg, 0.25mmol) in ethanol (10 mL). Reaction time 16 h. Yellow solid, yield 97 mg (78%). Anal. calcd. for $C_{34}H_{32}Cl_2N_7OPRu$: C, 53.90; H, 4.26; N, 12.94; Cl, 9.36. Found: C, 53.78; H, 4.35; N, 13.01; Cl, 9.42. HR-ESI-MS (methanol): $[M]^+$ m/z = 722.1160 (theoretical for $[C_{34}H_{32}ClN_7OPRu]^+$: m/z = 722.1138).IR (solid state): $\tilde{v}$/cm^{-1} = 3154w, 3140w, 3108w, 3061w, 2981w, 2927w, 2870w, 2822w, 1481w, 1435m, 1421w, 1405m, 1289m, 1278m, 1270m, 1250m, 1223w, 1099m, 1088m, 1062m, 1055m, 857m, 791m, 782m, 761m, 750m, 744m, 698s, 684w, 610m, 612m, 527s, 512m, 501m, 454m. ^{1}H NMR (CDCl$_3$): δ/ppm = 12.15 (s, 1H, C^{δ}H); 9.01, 8.76, 8.72 (d, 3H, $^3J_{HH}$ = 2.9 Hz, C^{γ}H); 8.02 (s-br, 2H, C^{1}H); 7.35 (t-br, 3H, C^{8}H); 7.33, 7.08, 6.59 (d, 3H, $^3J_{HH}$ = 2.2 Hz, C^{α}H); 7.17 (t, 6H, $^3J_{HH}$ = 7.70 Hz, C^{7}H); 6.99-6.94 (m, 8H, C^{6}H + C^{2}H); 6.30, 6.12, 6.03 (t, 3H, $^3J_{HH}$ = 2.6 Hz, C^{β}H), 4.74 (s, 2H, $^3J_{HH}$ = 4.8 Hz, C^{4}H); 3.66 (s-br, 1H, OH). ^{31}P{^{1}H} NMR (CDCl$_3$): δ/ppm = 50.1. ^{1}H NMR (CD$_3$OD): δ/ppm = 8.54, 8.50, 8.47 (d, 3H, $^3J_{HH}$ = 2.9 Hz, C^{γ}H); 8.04 (s-br, 2H, C^{1}H); 7.41 (t, 3H, $^3J_{HH}$ = 7.8 Hz, C^{8}H); 7.37, 7.11, 6.96 (d, 3H, $^3J_{HH}$ = 2.2 Hz, C^{α}H); 7.23 (t, 6H, $^3J_{HH}$ = 7.8 Hz, C^{7}H); 7.03 (d-br, 2H, C^{2}H); 7.00 (m, 6H, C^{6}H); 6.54, 6.34, 6.28 (t, 3H, $^3J_{HH}$ = 2.5 Hz, C^{β}H); 4.66 (s, 2H, C^{4}H);C^{δ}H and OH not detected. ^{13}C{^{1}H} NMR (CD$_3$OD): δ ppm = 157.1 (C^{1}br); 153.8, 151.0, 150.4 (C^α); 146.2 (C^3); 136.6, 135.9, 134.5 (C$_γ$); 135.1 (d, $^3J_{CP}$ = 9.4 Hz, C^7); 133.2 (d, $^1J_{CP}$ = 41.0 Hz, C^5); 131.3 (d, $^4J_{CP}$ = 2.3 Hz, C^8); 129.4 (d, $^2J_{CP}$ = 9.2 Hz, C^6); 122.7 (C^2); 110.3 (C^β); 109.7 (two C^β *superimposed*); 62.8 (C^4); 54.8 (C^δ). ^{31}P{^{1}H} NMR (CD$_3$OD): δ ppm = 50.6.Crystals suitable for X-ray diffraction were collected by slow evaporation of a CDCl$_3$ solution of **3**.

## [RuCl(κ^3-tpm)(PPh$_3$)(Py-EA)]Cl, 4 (Chart 7)

Chart 7. Structure of **4** (labelling refers to carbon atoms).
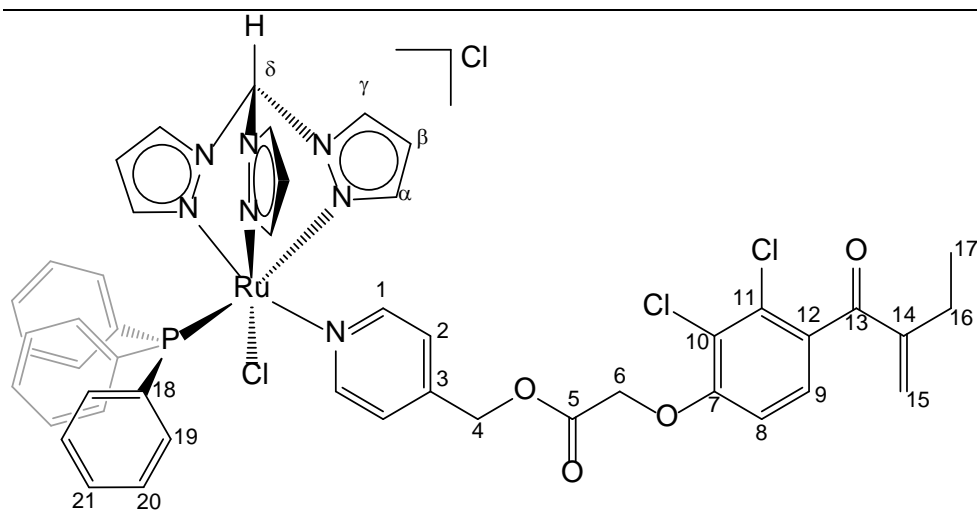
From **1** (150 mg, 0.16 mmol) and **Py-EA** (117 mg, 0.30 mmol) in anhydrous isopropanol (8 mL).

Reaction time: 8 h. Yellow solid, yield 134 mg (82%). Anal. calcd. for $C_{47}H_{42}Cl_4N_7O_4PRu$: C, 54.14; H, 4.06; N, 9.40; Cl, 13.60. Found: C, 54.02; H, 4.13; N, 9.31; Cl, 13.48. HR-ESI-MS (methanol): $[M]^+$ m/z = 1008.1141 (theoretical for $[C_{47}H_{42}Cl_3N_7O_4PRu]^+$: m/z = 1008.1177). IR (solid state): $\tilde{\upsilon}/cm^{-1}$ = 3106w, 3055w, 2963w, 2934w, 1756m ($\tilde{\upsilon}_{C=O}$), 1664m, 1582m, 1432m, 1407m, 1288m, 1251m, 1184m, 1121m,

1088s, 1055m, 997w, 856m, 784m, 750s, 694s, 607m, 529m, 509m, 500m, 456w. ^{1}H NMR (CD$_2$Cl$_2$): δ/ppm = 12.41 (s, 1H, C$^\delta$H); 9.02, 8.86, 8.77 (d, 3H, $^3J_{HH}$ = 2.9 Hz, C$^\gamma$H); 8.12 (s-br, 2H, C^{1}H); 7.36 (t, 3H, $^3J_{HH}$ = 7.2 Hz, C^{21}H); 7.30, 7.09, 6.68 (d, 3H, $^3J_{HH}$ = 2.2 Hz, C$^\alpha$H); 7.2-7.15 (m, 7H, C^{20}H + C^{9}H); 6.98 (t, 6H, $^3J_{HH}$ = 8.8 Hz, C^{19}H); 6.87-6.84 (m, 3H, C^{2}H + C^{8}H); 6.38, 6.17, 6.07 (t, 3H, $^3J_{HH}$ = 2.6 Hz, C$^\beta$H); 5.96, 5.57 (s, 2H, C^{15}H); 5.22 (s, 2H, C^{4}H); 4.88 (s, 2H, C^{6}H); 2.44 (q, 2H, $^3J_{HH}$ = 7.4 Hz, C^{16}H); 1.13 (t, 3H, $^3J_{HH}$ = 7.4 Hz, C^{17}H). ^{13}C{^{1}H} NMR (CD$_2$Cl$_2$): δ/ppm = 195.9 (C^{13}); 167.7 (C^5); 157.0 (br, C^1); 155.7 (C^7); 150.7 (C^{14}); 149.2, 148.7, 144.6 (C$^\alpha$); 144.8 (C^5); 136.3, 135.4, 134.3 (C$^\gamma$); 134.5 (C^{10}); 134.3 (d, $^3J_{CP}$ = 9.4 Hz, C^{19}); 132.5 (d, $^1J_{CP}$ = 40.6 Hz, C^{18}); 131.9 (C^{11}); 130.4 (d, $^5J_{CP}$ = 2.2 Hz, C^{21}); 129.2 (C^{15}); 128.7 (d, $^4J_{CP}$ = 9.2 Hz, C^{20}); 127.4 (C^9); 123.6 (C^{12}); 122.3 (C^2); 111.4 (C^8); 108.8, 108.7, 108.6 (C$^\beta$); 74.7 (C$^\delta$); 66.7 (C^4); 65.0 (C^6); 24.0 (C^{16}); 12.8 (C^{17}). ^{31}P{^{1}H} NMR (CD$_2$Cl$_2$): δ/ppm = 50.3.

[RuCl(κ³-tpm)(PPh₃)(Py-FLU)]Cl,5 (Chart 8)

**Chart 8**. Structure of **5**(labelling refers to carbon atoms).
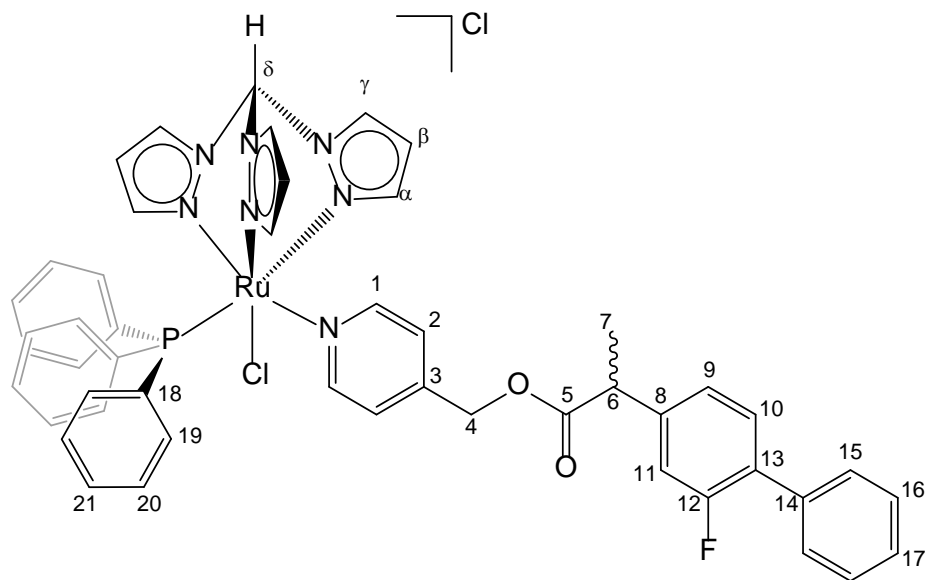
From **1** (150 mg, 0.16 mmol) and **Py-FLU** (100 mg, 0.30 mmol) in anhydrous isopropanol (8 mL).

Reaction time: 8 h. Yellow solid, yield 146 mg (90%). Anal. calcd. for $C_{49}H_{43}Cl_2FN_7O_2PRu$: C, 59.82;

H, 4.41; N, 9.97; Cl, 7.21. Found: C, 59.97; H, 4.36; N, 10.06; Cl, 7.27. HR-ESI-MS (methanol): $[M]^+$

m/z = 948.1935 (theoretical for $[C_{49}H_{43}ClFN_7O_2PRu]^+$: m/z =948.1964). IR (solid state): $\tilde{\upsilon}/cm^{-1}$ =

3107w, 3058w, 2988w, 2975w, 2905w, 2883w, 2761w, 2727w, 2681w, 2617w, 2589w, 2540w, 1737m

($\tilde{\upsilon}_{C=O}$), 1619w, 1583w, 1559w, 1513w, 1483m, 1449m, 1433, 1409m, 1382w, 1290m, 1253m, 1222m,

1183w, 1152w, 1133w, 1088s, 1061m, 1027w, 1010w, 999w, 989w, 922w, 855m, 789m, 764s, 750s,

724w, 695s, 609m, 527s, 512m, 502m, 456w. ^1H NMR (CD₂Cl₂): δ/ppm = 12.44 (s, 1H, $C^δH$); 9.01,

8.98 (d, 1H$_{A+B}$, $^3J_{HH}$ = 2.9 Hz, $C^γH$); 8.84, 8.76 (d-br, 2H, $C^γH$); 8.05 (s-br, 2H, C^1H); 7.48 (m, 2H,

$C^{15}H$); 7.44 (m, 1H, $C^{17}H$); 7.41 (m, 1H, $C^{10}H$); 7.40 (m, 2H, $C^{16}H$); 7.34 (m, 3H, $C^{21}H$); 7.29, 7.07 (d-

br, 2H, $C^αH$); 7.20-7.11 (m, 8H, $C^{20}H + C^9H + C^{11}H$); 6.96 (t, 6H, $^3J_{HH}$ = 8.8 Hz, $C^{19}H$); 6.75, 6.74 (d,

2H$_{A+B}$, $^3J_{HH}$ = 6.73 Hz, C^2H); 6.62, 6.60 (d, 1H$_{A+B}$, $^3J_{HH}$ = 2.3 Hz, $C^αH$); 6.35, 6.16 (t, 2H, $^3J_{HH}$ = 2.6

Hz, $C^βH$); 6.00, 5.94 (t, 1H$_{A+B}$, $^3J_{HH}$ = 2.6 Hz, $C^βH$); 5.16-5.05 (m, 2H, C^4H); 3.88 (q, 1H, $^3J_{HH}$ = 7.1

Hz, C^6H); 1.58 (d, 3H, $^3J_{HH}$ = 7.1 Hz, C^7H). Diastereoisomers ratio (A/B) = 1. $^{13}C\{^1H\}$ NMR (CD$_2$Cl$_2$): δ/ppm = 173.7 (C^5); 159.1 (d, C^{12}, $^1J_{CF}$ = 247.9 Hz); 156.8 (*br*, C^1); 149.2, 148.8, 144.7 ($C^α$);146.0 (C^3); 142.1 (d, C^8,$^3J_{CF}$ = 7.7 Hz); 136.4, 135.5, 134.3 ($C^γ$); 135.8 (d, C^{14}, $^3J_{CF}$ = 1.2 Hz); 134.4 (C^{19}, $^2J_{CP}$ = 9.5 Hz); 132.6 (C^{18}, $^1J_{CP}$ = 40.5 Hz); 131.5 (C^{10}, $^3J_{CF}$ = 3.8 Hz); 130.5 (C^{21}, $^4J_{CP}$ = 2.1 Hz); 129.4 (d, C^{15}, $^4J_{CF}$ = 2.8 Hz); 129.1 (C^{17}); 128.8 (d, C^{20}, $^2J_{CP}$ = 9.2 Hz); 128.6 (d, C^{13}, $^2J_{CF}$ = 13.6 Hz); 128.5 (d, C^{16}, $^5J_{CF}$ = 2.7 Hz); 124.4, 124.3 (d, C^9, $^4J_{CF}$ = 3.3 Hz); 122.2 (C^2); 115.9, 115.6 (d, C^{11}, $^2J_{CF}$ = 23.8 Hz); 108.9, 108.8, 108.6 ($C^β$); 74.8 ($C^δ$); 64.4 (C^4); 45.4 (d, C^6_{A+B},$^4J_{CF}$ = 1.5 Hz); 18.6 (d, C^7).$^{31}P\{^1H\}$ NMR (CD$_2$Cl$_2$): δ/ppm = 50.3. ^{19}F NMR (CD$_2$Cl$_2$): δ ppm = -117.9.

[RuCl(κ^3-tpm)(PPh$_3$)(Py-IBU)]Cl, 6 (Chart 9)

Chart 9. Structure of **6**(labelling refers to carbon atoms).
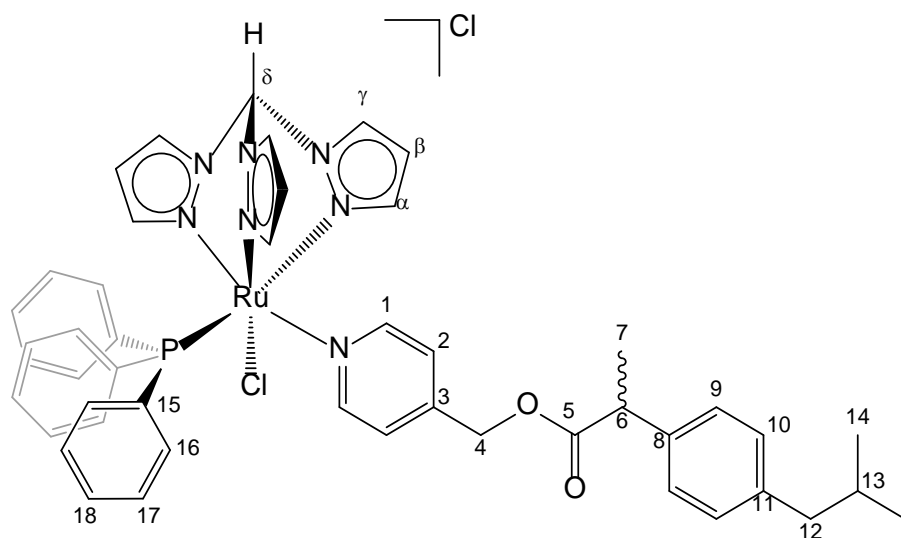
From **1** (150 mg, 0.160 mmol) and **Py-IBU** (84 mg, 0.30 mmol) in anhydrous isopropanol (8 mL). Reaction time: 8 h. Yellow solid, yield 146 mg (90%). Anal. calcd. for C$_{47}$H$_{48}$Cl$_2$N$_7$O$_2$PRu: C, 59.68; H, 5.11; N, 10.37; Cl, 7.50. Found: C, 59.52; H, 5.19; N, 10.28; Cl, 7.56.HR-ESI-MS (methanol): [M]$^+$ m/z = 910.2343 (theoretical for [C$_{47}$H$_{48}$ClN$_7$O$_2$PRu]$^+$: m/z =910.2371).IR (solid state): ṽ/cm^{-1} = 3129w, 3107w, 3055w, 2957w, 2914w, 2868w, 1739m (ṽ$_{C=O}$), 1618w, 1508w, 1482w, 1452w, 1435w,

1406m, 1379w, 1290m, 1253m, 1176w, 1157w, 1088m, 1050w, 984w, 857m, 814w, 792w, 780w, 751s, 698s, 683w, 605w, 529s, 504s, 455m. ^{1}H NMR (CD$_2$Cl$_2$): δ/ppm = 12.43 (s, 1H, C$^\delta$H); 9.03, 9.02 (d, 1H$_{A+B}$, $^3J_{HH}$ = 2.5, C$^\gamma$H); 8.85, 8.77 (d, 2H, $^3J_{HH}$ = 2.8, C$^\gamma$H); 8.02 (s-br, 2H, C^{1}H); 7.35 (t, 3H, $^3J_{HP}$ = 7.4 Hz, C^{18}H); 7.28, 7.07, 6.63 (d, 3H, $^3J_{HH}$ = 2.2 Hz, C$^\alpha$H); 7.19 (m, 2H, C^{10}H); 7.17 (t-br, 6H, C^{17}H); 7.09 (m, 2H, C^{9}H); 6.95 (t, 6H, $^3J_{HP}$ = 8.8 Hz, C^{16}H); 6.69 (d, 1H, C^{2}H); 6.37, 6.16 (t, 2H, $^3J_{HH}$ = 2.6 Hz, C$^\beta$H); 6.08, 6.07 (t, 1H$_{A+B}$, $^3J_{HH}$ = 2.9 Hz, C$^\beta$H); 5.13-5.00 (m, 2H$_{A+B}$, C^{4}H); 3.80 (q, 1H$_{A+B}$, $^3J_{HH}$ = 7.1 Hz, C^{6}H); 2.42 (d, 2H, $^3J_{HH}$ = 7.1 Hz, C^{12}H); 1.78 (m, 1H, C^{13}H); 1.53, 1.52 (d, 3H$_{A+B}$, $^3J_{HH}$ = 7.1 Hz, C^{7}H); 0.87, 0.84 (d, 6H$_{A+B}$, $^3J_{HH}$ = 6.6, Hz, C^{14}H). Diastereoisomers ratio (A/B) = 1. ^{13}C{^{1}H} NMR (CD$_2$Cl$_2$): δ/ppm = 174.4 (C^5); 156.6 (br, C^1); 149.2, 148.7, 144.7 (C$^\alpha$); 146.3 (C^3); 141.6 (C^{11}); 137.9 (C^8); 136.3, 135.4, 134.2 (C$^\gamma$); 134.3 (d, $^2J_{CP}$ = 9.4 Hz, C^{16}); 132.6 (d, $^1J_{CP}$ = 40.6 Hz, C^{15}); 130.4 (d, $^4J_{CP}$ = 2.5 Hz, C^{18}); 123.0 (C^9); 128.8 (d, $^3J_{CP}$ = 9.2 Hz, C^{17}); 127.8 (C^{10}); 122.0 (C^2); 108.8, 108.7, 108.6(C$^\beta$); 74.8 (C$^\delta$); 64.1 (C^4); 45.5 (C^6); 45.4 (C^{12}); 30.8 (C^{13}); 22.6 (C^{14}); 18.7, 18.6 (C$^7_{A+B}$). ^{31}P{^{1}H} NMR (CD$_2$Cl$_2$): δ/ppm = 50.3.

[RuCl(κ^3-tpm)(PPh$_3$)(Py-NAP)]Cl, 7 (Chart 10)

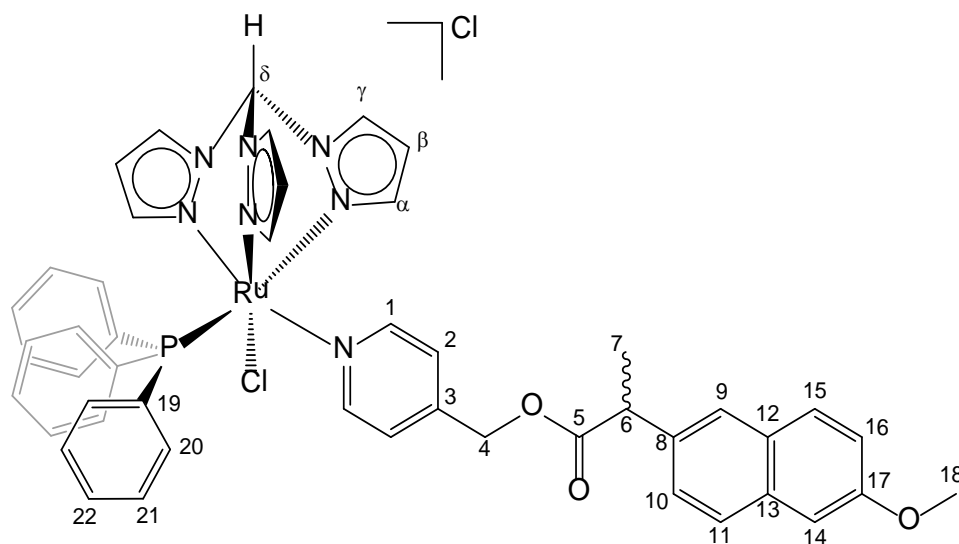**Chart 10**. Structure of **7**(labelling refers to carbon atoms).

From **1** (150 mg, 0.160 mmol) and **Py-NAP** (96 mg, 0.30 mmol) in anhydrous isopropanol (8 mL). Reaction time: 8 h. Yellow solid, yield 132 mg (82%). Anal. calcd. for $C_{48}H_{44}Cl_2N_7O_3PRu$: C, 59.44; H, 4.57; N, 10.11; Cl, 7.31. Found: C, 59.31; H, 4.64; N, 10.03; Cl, 7.24. HR-ESI-MS (methanol): $[M]^+$ m/z = 934.1985 (theoretical for $[C_{48}H_{44}ClN_7O_3PRu]^+$: m/z = 934.2008).IR (solid state): $\tilde{\upsilon}/cm^{-1}$ = 3110w, 3052w, 2975w, 2935w, 1736m ($\tilde{\upsilon}_{C=O}$), 1633w, 1606m, 1506w, 1484m, 1454m, 1434m, 1409m, 1288m, 1270m, 1255m, 1223m, 11774m, 1154m, 1090s, 1053m, 1027m, 999w, 983w, 924w, 890w, 856w, 812w, 790s, 749s, 696s, 609m, 528s, 511m, 501m, 476w. ^{1}H NMR (CD_2Cl_2): δ/ppm = 12.35 (s, 1H, $C^\delta H$); 9.00 (d, 1H, $^3J_{HH}$ = 2.5, $C^\gamma H$); 8.82 (m, 1H, $^3J_{HH}$ = 2.7, $C^\gamma H$); 8.76 (d, 1H, $^3J_{HH}$ = 2.8, $C^\gamma H$); 7.99 (s-br, 2H, C^1H); 7.71 (d, 1H, $^3J_{HH}$ = 7.7, $C^{11}H$); 7.70-7.67 (m, 2H, C^9H + $C^{15}H$); 7.39 (d, 1H, $^3J_{HH}$ = 8.5 Hz, $C^{10}H$); 7.32 (m, 3H, $C^{22}H$); 7.25 (d, 1H, $^3J_{HH}$ = 2.1 Hz, $C^\alpha H$); 7.17-7.12 (m, 8H, $C^{21}H$ + $C^{16}H$ + $C^{14}H$); 7.07 (d, 1H, $^3J_{HH}$ = 2.2 Hz, $C^\alpha H$); 6.94 (t, 6H, $^3J_{HP}$ = 8.8 Hz, $C^{20}H$); 6.72, 6.70 (d, $2H_{A+B}$, C^2H); 6.58, 6.54 (d, $1H_{A+B}$, $^3J_{HH}$ = 2.3, $C^\alpha H$); 6.34 (t-br, 1H,$C^\beta H$); 6.16 (t, 1H, $^3J_{HH}$ = 2.5 Hz, $C^\beta H$); 6.05, 6.04 (m, $1H_{A+B}$, $C^\beta H$); 5.13-5.02 (m, 2H, C^4H); 3.97 (q, 1H, $^3J_{HH}$ = 7.2 Hz, C^6H); 3.90 (s, 3H, $C^{18}H$); 1.62, 1.60 (d, 3H, $^3J_{HH}$ = 7.1 Hz, C^7H). Diastereoisomers ratio(A/B)= 1. $^{13}C\{^1H\}$ NMR (CD_2Cl_2): δ/ppm = 174.4 (C^5); 158.4 (C^{17}); 156.7 (br, C^1); 149.2, 148.7, 144.6 (C^α); 146.2 (C^3); 136.3, 135.4, 134.2 (C^γ); 135.8, 135.7 (C^8_{A+B}); 134.4 (C^{13}); 134.3 (d, $^2J_{CP}$ = 9.4 Hz, C^{20}); 132.6 (d, $^1J_{CP}$ = 40.5 Hz, C^{19}); 130.4 (d, $^4J_{CP}$ = 1.8 Hz, C^{22}); 129.7 (C^{15}); 129.4 (C^{12}); 128.7 (d, $^3J_{CP}$ = 9.3 Hz, C^{21});127.8 (C^{11}); 126.7 (C^{10}); 126.5 (C^9); 122.1 (C^2); 119.7 (C^{16});108.8, 108.7, 108.6 (C^β); 106.1 (C^{14}); 74.8 (C^δ); 64.2 (C^4); 55.9 (C^{18}); 45.9 (C^6); 18.7 (C^7). $^{31}P\{^1H\}$ NMR (CD_2Cl_2): δ/ppm = 50.3.

3. X-ray crystallography

Crystal data and collection details for **2**·CH_2Cl_2·$2H_2O$and **3**·$3CHCl_3$ are reported in Table 5. Data were recorded on a Bruker APEX II diffractometer equipped with a PHOTON2 detector using Mo–Kα radiation. The structures were solved by direct methods and refined by full-matrix least-squares based

on all data using F^2.[67] Hydrogen atoms were fixed at calculated positions and refined using a riding model.

Table 5. Crystal data and measurement details for **2**·CH_2Cl_2·$2H_2O$ and **3**·$3CHCl_3$.

	2·CH_2Cl_2·$2H_2O$	**3**·$3CHCl_3$
Formula	$C_{34}H_{36}Cl_4N_7O_2PRu$	$C_{37}H_{35}Cl_{11}N_7OPRu$
FW	848.54	1115.71
T, K	100(2)	100(2)
λ, Å	0.71073	0.71073
Crystal system	Triclinic	Triclinic
Space group	$P\bar{1}$	$P\bar{1}$
a, Å	9.7635(4)	13.9551(5)
b, Å	10.1639(5)	15.8845(7)
c, Å	19.2737(8)	21.0285(8)
α,°	98.1590(10)	98.9100(10)
β,°	104.1840(10)	92.5850(10)
γ,°	96.3230(10)	91.9650(10)
Cell Volume, Å^3	1814.51(14)	4596.4(3)
Z	2	4
D_c, g·cm^{-3}	1.553	1.612
μ, mm^{-1}	0.813	1.055
F(000)	864	2240
Crystal size, mm	0.16×0.14×0.10	0.16×0.15×0.11
θ limits,°	2.150-26.000	1.719-25.250
Reflections collected	33241	61332
Independent reflections	7088 [R_{int} = 0.0901]	16602 [R_{int} = 0.0356]
Data / restraints /parameters	7088 / 40 / 454	16602 / 0 / 1047
Goodness on fit on F$^{2\ a}$	1.052	1.081
R_1 ($I > 2\sigma(I)$) ^{b}	0.0541	0.0503
wR_2 (all data) ^{c}	0.1553	0.1278
Largest diff. peak and hole, e Å^{-3}	2.448 / −1.694	2.328 / −1.019

^{a} Goodness on fit on F^2 = $[\Sigma w(F_O^2 - F_C^2)^2/(N_{ref} - N_{param})]^{1/2}$, where $w = 1/[\sigma^2(F_O^2) + (aP)^2 + bP]$, where $P = (F_O^2 + 2F_C^2)/3$; N_{ref} = number of reflections used in the refinement; N_{param} = number of refined parameters. ^{b} R$_1$ = $\Sigma||F_O| - |F_C||/\Sigma|F_O|$. ^{c} wR$_2$ = $[\Sigma w(F_O^2 - F_C^2)^2/\Sigma w(F_O^2)^2]^{1/2}$, where $w = 1/[\sigma^2(F_O^2) + (aP)^2 + bP]$, where $P = (F_O^2 + 2F_C^2)/3$.

4. Behaviour in aqueous media

a) Solubility in water. A suspension of the selected ruthenium complex (3-5 mg) in a D_2O solution (0.7 mL) containing Me_2SO_2 as internal standard (3.36·10^{-3} M) was vigorously stirred at 21 °C for 3 h.

The resulting saturated solution was filtered over celite, transferred into an NMR tube and analysed by ^{1}H NMR spectroscopy (delay time = 3 s; number of scans = 20). The concentration (solubility) was calculated by the relative integral (starting complex + aquo-complex) with respect to Me$_2$SO$_2$ (δ/ppm = 3.14). Results are compiled in Table 2.

b) Octanol/water partition coefficients (Log P_{ow}). Partition coefficients (P_{ow}; IUPAC: K_D partition constant[68]), defined as $P_{ow} = c_{org}/c_{aq}$, where c_{org} and c_{aq} are molar concentrations of the selected compound in the organic and aqueous phase, respectively, were determined by the shake-flask method and UV-Vis measurements.[52,69] Deionized water and 1-octanol were vigorously stirred for 24 h, to enable saturation of both phases, then separated by centrifugation. A stock solution of the selected ruthenium compound (*ca.* 2 mg) was prepared by first adding DMSO, (50 µL, to help solubilization), followed by octanol-saturated water (2.5 mL). The solution was diluted with octanol-saturated water (*ca.* 1:3 *v/v* ratio, $c_{Ru} \approx 10^{-4}$ M, so that $1.5 \le A \le 2.0$ at λ_{max}) and its UV-Vis spectrum was recorded (A^0_{aq}). An aliquot of the solution (V_{aq} = 1.2 mL) was transferred into a test tube and water-saturated octanol ($V_{org} = V_{aq}$ = 1.2 mL) was added. The mixture was vigorously stirred for 20 min at 21 °C then centrifuged (5000 rpm, 5 min). The UV-Vis spectrum of the aqueous phase was recorded (A^f_{aq}) and the partition coefficient was calculated as $P_{ow} = (A^0_{aq} - A^f_{aq})/A^f_{aq}$ where A^0_{aq} and A^f_{aq} are the absorbance in the aqueous phase before and after partition with the organic phase, respectively.[69c] For **1**, an inverse procedure was followed, starting from a solution of the compound in water-saturated octanol. The partition coefficient was calculated as $P_{ow} = A^f_{org}/(A^0_{org} - A^f_{org})$ where A^0_{org} and A^f_{org} are the absorbance in the organic phase before and after partition with the aqueous phase, respectively. The wavelength of the maximum absorption of each compound (280 - 380 nm range) was used for UV-Vis quantitation. The procedure was repeated three times for each sample (from the same stock solution); results are given as mean ± standard deviation (Table 2). Naphthoquinone was used as a reference compound (Log P_{ow}= 1.8 ± 0.2; literature: 1.71[70]).

c) Stability in D_2O and DMSO-d_6/D_2O. The same samples prepared at point a) (complexes **2** and **3**) were used in this experiment. In addition, all complexes were analysed in D_2O mixtures containing additional deuterated solvents. The selected ruthenium complex (2 mg) was dissolved in DMSO-d_6/D_2O 4:1 v/v solution (0.75 mL)containing Me_2SO_2 as standard.[71] The resulting solution was stirred at 21 °C for 5 min, filtered over celite, transferred into an NMR tube, analysed by ^1H NMR and ^{31}P NMR spectroscopy(delay time = 3 s; number of scans = 20)and then heated at 37 °C for 48 h. After cooling to room temperature, NMR analyses were repeated. The percentages of starting complex, related aquo complex and complex **8**were calculated by signal integrations with respect to Me_2SO_2 (c = $3.3\cdot10^{-3}$ mol·L^{-1}; δ/ppm = 3.14 in D_2O; δ/ppm = 2.95 in DMSO-d_6/D_2O 4:1 v/v; see Table 2 and Table S1).

d) Stability in cell culture medium. Powdered DMEM cell culture medium (1000 mg/L glucose and L-glutamine, without sodium bicarbonate and phenol red; D2902 - Merck) was dissolved in D_2O (10 mg/mL), according to the manufacturer's instructions. The solution of deuterated cell culture medium ("DMEM-d") was treated with Me_2SO_2 ($6.6\cdot10^{-3}$ M) and NaH_2PO_4 / Na_2HPO_4 (0.15 M, pD = 7.5[72]), then stored at 4 °C under N_2. The same procedure reported at point c) was followed for the preparation and analysis of the samples, using DMEM-d instead of D_2O.The percentages of starting complex, related aquo complex or complex **8**were calculated by signal integrations with respect to Me_2SO_2 (δ/ppm = 3.16 in DMSO-d_6/DMEM-d 1:4 and 1:3 v/v; δ/ppm = 2.95 in DMSO-d_6/DMEM-d 4:1 v/v).

e) Conductivity measurements. Complex **3** (7.5 mg) was dissolved in 10 mL of pureH_2O (final concentration of 10^{-3} M). The solution was heated at 37° C and the conductivity was monitored over 24h.

f) ESI-MS. Solutions were prepared by dissolving complexes at a concentration of 10^{-3} M in methanol and analysed as soon as the solutions was prepared. Complex **3** was also analysed in H_2O solution (10^{-3} M) immediately after the preparation of the sample and 3h after from the preparation.

5. Cell culture and cytotoxicity studies

Human ovarian carcinoma (A2780 and A2780cisR) cell lines were obtained from the European Collection of Cell Cultures. The human embryonic kidney (HEK-293T) cell line was obtained from ATCC (Sigma, Buchs, Switzerland). RPMI 1640 GlutaMAX (where RPMI = Roswell Park Memorial Institute), and DMEM GlutaMAX media (where DMEM = Dulbecco's modified Eagle medium) were obtained from Life Technologies, and fetal bovine serum (FBS) was obtained from Sigma. The cells were cultured in RPMI 1640 GlutaMAX (A2780 and A2780cisR) and DMEM GlutaMAX (HEK-293T) media containing 10% heat-inactivated FBS at 37 °C and CO_2 (5%). The A2780cisR cell line was routinely treated with cisplatin (1 µM) in the media to maintain cisplatin resistance. The cytotoxicity was determined using the 3-(4,5-dimethyl 2-thiazolyl)-2,5-diphenyl-2H-tetrazolium bromide (MTT) assay.[73] Cells were seeded in flat-bottomed 96-well plates as a suspension in a prepared medium (100 µL aliquots and approximately 4300 cells/well) and preincubated for 24 h. Stock solutions of compounds were prepared in DMSO and were diluted in the medium. The solutions were sequentially diluted to give a final DMSO concentration of 0.5% and a final compound concentration range (0−200 µM). Cisplatin and RAPTA-C were tested as positive (0−100 µM) and negative (200 µM) controls respectively. The compounds were added to the preincubated 96-well plates in 100 µL aliquots, and the plates were incubated for a further 72 h. MTT (10 µL, 5 mg/mL in Dulbecco's phosphate-buffered saline) was added to the cells, and the plates were incubated for a further 4 h. The culture medium was aspirated and the purple formazan crystals, formed by the mitochondrial dehydrogenase activity of vital cells, were dissolved in DMSO (100 µL/well). The absorbance of the resulting solutions, directly proportional to the number of surviving cells, was quantified at 590 nm using a SpectroMax M5e multimode microplate reader (using SoftMax Pro software, version 6.2.2). The percentage of surviving cells was calculated from the absorbance of wells corresponding to the untreated control cells. The reported IC_{50} values are based on the means from two independent experiments, each comprising four tests per concentration level.

6. Enzyme activity assays

The enzymatic activity of COX-2 (0.25 UN) was fluorimetrically assayed at 576 nm/586 nm and at 25ºC by measuring the rate of arachidonic acid (ARA) conjugation with COX-2 as a function of time, by using a protocol reported earlier.[36] The assay mixture contained 25 μM ADHP, 5 μM hemin, and 37.5 μM ARA in 0.1 M of Tris-HCl buffer at pH 8. The inhibitory efficacy of flurbiprofen, ibuprofen, naproxen, PyOH, Py-FLU, Py-IBU, and Py-NAP were determined by recording the residual activity of COX-2 in the presence of variable concentrations of the analysed compounds (25μM - 3000 μM).

The enzymatic activity of GST P1 (20 nM) was spectrophotometrically assayed at 340 nm at 37ºC by measuring the CDNB–GSH (1- chloro-2,4-dinitrobenzene-glutathione) conjugation rate as a function of time, by using a protocol reported earlier.[62] The assay mixture contained 1 mM CDNB (1-chloro-2,4-dinitrobenzene) and 2 mM GSH (glutathione) of 0.1 M of potassium phosphate buffer at pH 6.5. The inhibitory efficacy of ethacrynic acid, PyOH, and Py-EA were determined by recording the residual activity of GST P1 in the presence of variable concentrations of the analysed compounds (1μM - 500 μM). The IC_{50} value for each compound was obtained using GraphPad Prism 7 software. All the inhibitor assays were performed at least in triplicate, for both enzymes.

Supporting Information Available

IR and NMR spectra of products; NMR data of ruthenium complexes in aqueous solutions; biological data; HR-ESI-MS spectra of **3** in H$_2$O; X-ray data concerning hydrogen bonds in the structures of **2** and

3.CCDC reference numbers 2193265(**2**) and2193266(**3**) contain the supplementary crystallographic data for the X-ray studies reported in this work. These data are available free of charge at http://www.ccdc.cam.ac.uk/structures. Authors will release the atomic coordinates upon article publication.

The authors declare no competing financial interests.

References

1   Anthony, E. J.; Bolitho, E. M.; Bridgewater, H. E.; Carter, O. W. L.; Donnelly, J. M.; Imberti, C.; Lant, E. C.; Lermyte, F.; Needham, R. J.; Palau, M.; Sadler, P. J.; Shi, H.; Wang, F.-X.; Zhang, W.-Y.; Zhang, Z. Metallodrugs are unique: opportunities and challenges of discovery and development. Chem. Sci., 2020, 11, 12888–12917.

2   Marloye, M.; Berger, G.; Gelbcke, M. A survey of the mechanisms of action of anticancer transition metal complexes. Future Med. Chem. 2016, 8, 2263-2286.

3   Boros, E.; Dyson, P. J.; Gasser, G. Classification of metal-based drugs according to their mechanisms of action. Chem 2020, 6, 41–60.

4   Qi, L.; Luo, Q.; Zhang, Y.; Jia, F.; Zhao, Y.; Wang, F. Advances in Toxicological Research of the Anticancer Drug Cisplatin, Chem. Res. Toxicol. 2019, 32, 1469−1486

5   Oun, R.; Moussa, Y. E.; Wheate, N. J. The side effects of platinum-based chemotherapy drugs: a review for chemists, Dalton Trans. 2018, 47, 6645.

6   Yu, C.; Wang, Z.; Sun, Z.; Zhang, L.; Zhang, W.; Xu, Y.; Zhang, J.-J. Platinum-Based Combination Therapy: Molecular Rationale, Current Clinical Uses, and Future Perspectives. J. Med. Chem. 2020, 63, 13397-13412.

7   Murray, B. S.; Dyson, P. J. Recent progress in the development of organometallics for the treatment of cancer. Current Opinion Chem. Biol. 2020, 56, 28-34.

8   S. M. Meier-Menches, C. Gerner, W. Berger, C. G. Hartinger, B. K. Keppler, Chem. Soc. Rev. 2018, 47, 909.

9   Murray, B. S.; Babak, M. V.; Hartinger, C. G.; Dyson, P. J. The development of RAPTA compounds for the treatment of tumors, Coord. Chem. Rev. 2016, 306, 86–114.

10   Bergamo, A.; Masi, A.; Peacock, A. F. A.; Habtemariam, A.; Sadler, P. J.; Sava, G. In vivo tumor and metastasis reduction and in vitro effects on invasion assays of the ruthenium RM175 and osmium AFAP51 organometallics in the mammary cancer model, J. Inorg. Biochem. 2010, 104, 79-86.

11   Kumar Singh, A.; Pandey, D. S.; Xu, Q.; Braunstein, P. Recent advances in supramolecular and biological aspects of arene ruthenium(II) complexes. Coord. Chem. Rev. 2014, 270–271, 31–56.

12   Swaminathan, S.; Haribabu, J.; Balakrishnan, N.; Vasanthakumar, P.; Karvembu, R. Piano stool Ru(II)-arene complexes having three monodentate legs: A comprehensive review on their development as anticancer therapeutics over the past decade. Coord. Chem. Rev. 2022, 459, 214403.

13   Guerriero, A.; Oberhauser, W.; Riedel, T.; Peruzzini, M.; Dyson, P. J.; Gonsalvi, L. New class of half-sandwich ruthenium (II) arene complexes bearing the water-soluble CAP ligand as an in vitro anticancer agent, Inorg. Chem. 2017, 56, 10, 5514–5518.

14   Chotard, F.; Malacea-Kabbara, R.; Balan, C.; Bodio, E.; Picquet, M.; Richard, P.; Ponce-Vargas, M.; Fleurat-Lessard, P.; Le Gendre, P. Atom transfer radical addition catalyzed by ruthenium-arene complexes bearing a hybrid phosphine-diene ligand, Organometallics 2018, 37, 812-820.

15   Biancalana, L.; Pampaloni, G.; Zacchini, S.; Marchetti, F. Synthesis, characterization and behavior in water/DMSO solution of Ru(II) arene complexes with bioactive carboxylates. J. Organomet. Chem. 2018, 869, 201-211.

16   Egger, A. E.; Hartinger, C. G.; Renfrew, A. K.; Dyson, P. J. Metabolization of [Ru(η^6-C$_6$H$_5$CF$_3$)(pta)Cl$_2$]: a cytotoxic RAPTA-type complex with a strongly electron withdrawing arene ligand. J Biol Inorg Chem 2010, 15, 919–927.

17   Bugarcic, T.; Habtemariam, A.; Stepankova, J.; Heringova, P.; Kasparkova, J.; Deeth, R. J.; Johnstone, R. D. L.; Prescimone, A.; Parkin, A.; Parsons, S.; Brabec, V.; Sadler, P. J. The contrasting chemistry and cancer cell cytotoxicity of bipyridine and bipyridinediol ruthenium(II) arene complexes. Inorg. Chem. 2008, 47, 11470-11486.

18   Štarha, P.; Trávníček, Z. Non-platinum complexes containing releasable biologically active ligands, Coord. Chem. Rev. 2019, 395, 130–145.

19   Gibson, D. Platinum(IV) anticancer agents; are we en route to the holy grail or to a dead end? J. Inorg. Biochem. 2021, 217, 111353.

20   Hanif, M.; Hartinger, C. G. From the hypothesis-driven development of organometallic anticancer drugs to new methods in mode of action studies, Advances in Inorganic Chemistry, Elsevier Ed., 2020, Vol. 75, 2020, 339-359.

21   Das, P.; Delost, M. D.; Qureshi, M. H.; Smith, D. T.; Njardarson, J. T. A Survey of the Structures of US FDA Approved Combination Drugs, J. Med. Chem. 2019, 62, 4265 – 4311.

22   Clavel, C. M.; Paunescu, E.; Nowak-Sliwinska, P.; Griffioen, A. W.; Scopelliti, R.; Dyson, P. J. Modulating the Anticancer Activity of Ruthenium(II) – Arene Complexes, J. Med. Chem. 2015, 58, 3356−3365.

23   Steel, T. R.; Walsh, F.; Wieczorek-Błauz, A.; Hanif, M.; Hartinger, C. G. Monodentately-coordinated bioactive moieties in multimodal half-sandwich organoruthenium anticancer agents. Coord. Chem. Rev. 2021, 439, 213890, and references therein.

24   Bigmore, H. R.; Lawrence, S. C.; Mountford, P.; Tredget, C. S. Coordination, organometallic and related chemistry of tris(pyrazolyl)methane ligands. Dalton Trans. 2005, 635–651.

25   Reger, D. L. Tris(pyrazolyl)methane ligands: the neutral analogs of tris(pyrazolyl)borate ligands. Comments on Inorganic Chemistry 1999, 21, 1-28.

26   Munoz-Molina, J. M.; Belderrain, T. R.; Perez, P. J. Group 11 tris(pyrazolyl)methane complexes: structural features and catalytic applications. Dalton Trans. 2019, 48, 10772-10781.

27   Martins, L. M.D.R.S.; Pombeiro, A. J. L.; Tris(pyrazol-1-yl)methane metal complexes for catalytic mild oxidative functionalizations of alkanes, alkenes and ketones. Coord. Chem. Rev. 2014, 265, 74–88..

28   Martins, L.M.D.R.S. C-scorpionate complexes: Ever young catalytic tools. Coord. Chem. Rev. 2019, 396, 89–102.

29   B. Serli, E. Zangrando, T. Gianferrara, C. Scolaro, P. J. Dyson, A. Bergamo, E. Alessio, Is the Aromatic Fragment of Piano-Stool Ruthenium Compounds an Essential Feature for Anticancer Activity? The Development of New RuII-[9]aneS3Analogues, Eur. J. Inorg. Chem. 2005, 3423–3434.

30   A. Rilak, I. Bratsos, E. Zangrando, J. Kljun, I. Turel, Z. D. Bugarčić, E. Alessio, Factors that influence the antiproliferative activity of half sandwich RuII–[9]aneS3 coordination compounds: activation kinetics and interaction with guanine derivatives, Dalton Trans., 2012, 41, 11608–11618.

31   Walker, J. M.; McEwan, A.; Pycko, R.; Tassotto, M. L.; Gottardo, C.; Th'ng, J.; Wang, R.; Spivak, G. J. [Tris(pyrazolyl)methane]ruthenium complexes capable of inhibiting cancer cell growth. Eur. J. Inorg. Chem. 2009, 4629–4633.

32   Cervinka, J.; Gobbo, A.; Biancalana, L.; Markova, L.; Novohradsky, V.; Guelfi, M.; Zacchini, S.; Kasparkova, J.; Brabec, V.; Marchetti, F. Ruthenium(II) Tris-Pyrazolylmethane Complexes Inhibit Cancer Cell Growth by Disrupting Mitochondrial Calcium Homeostasis, J. Med. Chem. 2022, J. Med. Chem. 2022, 65, 10567−10587.

33   Ang, W. H.; Khalaila, I.; Allardyce, C. S.; Juillerat-Jeanneret, L.; Dyson, P. J. Rational Design of Platinum(IV) Compounds to Overcome Glutathione-S-Transferase Mediated Drug Resistance, J. Am. Chem. Soc. 2005, 127, 1382-1383.

34   Păunescu, E.; Soudani, M.; Martin, P.; Scopelliti, R.; Lo Bello, M.; Dyson, P. J. Organometallic Glutathione S- Transferase Inhibitors, Organometallics 2017, 36, 3313−3321.

35   Ang, W. H.; Parker, L. J.; De Luca, A.; Juillerat-Jeanneret, L.; Morton, C. J.; Lo Bello, M.; Parker, M. W.; Dyson, P. J. Rational Design of an Organometallic Glutathione Transferase Inhibitor, Angew. Chem. Int. Ed. 2009, 48, 3854 –3857.

36   Biancalana, L.; Kostrhunova, H.; Batchelor, L. K.; Hadiji, M.; Degano, I.; Pampaloni, G.; Zacchini, S.; Dyson, P. J.; Brabec, V.; Marchetti, F. Hetero-Bis-Conjugation of Bioactive Molecules to Half-Sandwich Ruthenium(II) and Iridium(III) Complexes Provides Synergic Effects in Cancer Cell Cytotoxicity. Inorg. Chem. 2021, 60, 9529 – 9541.

37   Biancalana, L.; Batchelor, L. K.; Pereira, S. A. P.; Tseng, P.-J.; Zacchini, S.; Pampaloni, G.; Saraiva, L. M. F. S.; Dyson, P. J.; Marchetti, F. Bis-conjugation of Bioactive Molecules to Cisplatin-like Complexes through (2,2'-Bipyridine)-4,4'-Dicarboxylic Acid with Optimal Cytotoxicity Profile Provided by the Combination Ethacrynic Acid/Flurbiprofen, Chem. Eur. J. 2020, 26, 17525 – 17535.

38   Tabrizi, L.; Romanova, J. Antiproliferative Activity of Gold(I) N-Heterocyclic Carbene and Triphenylphosphine Complexes with Ibuprofen Derivatives as Effective Enzyme Inhibitors, Appl Organometal Chem. 2020;34:e5618.

39   Benadiba, M.; Rolim Prudente dos Santos, R.; de Oliveira Silva, D.; Colquhoun, A. Inhibition of C6 rat glioma proliferation by [Ru2Cl(Ibp)4] depends on changes in p21, p27, Bax/Bcl2 ratio and mitochondrial membrane potential, J. Inorg. Biochem. 2010, 104, 928–935.

40 Biancalana, L.; Batchelor, L. K.; De Palo, A.; Zacchini, S.; Pampaloni, G.; Dyson, P. J.; Marchetti, F. A general strategy to add diversity to ruthenium arene complexes with bioactive organic compounds via a coordinated (4-hydroxyphenyl)diphenylphosphine ligand. Dalton Trans., 2017, 46, 12001–12004.

41 Deb, J.; Ranjan Lakshman, T.; Ghosh, I.; Sankar Janab, S.; Kanti Paine, T. Mechanistic studies of in vitro anti-proliferative and anti-inflammatory activities of the Zn(ii)–NSAID complexes of 1,10-phenanthroline-5,6-dione in MDA-MB-231 cells, Dalton Trans., 2020, 49, 11375-11384.

42 Srivastava, P.; Singh, K.; Verma, M.; Sivakumar, S.; Patra, A. K. Photoactive platinum(II) complexes of nonsteroidal anti-inflammatory drug naproxen: Interaction with biological targets, antioxidant activity and cytotoxicity, Eur. J. Med. Chem. 2018, 144, 243-254.

43 Abdel-Aziz, A. A.-M.; Al-Badr, A. A.; Hafez, G. A. Flurbiprofen, in "Profiles of Drug Substances, Excipients, and Related Methodology", 2012, Volume 37, Elsevier Ed.

44 Rainsford, K. D. Ibuprofen: pharmacology, therapeutics and side effects, Springer Science & Business Media, Springer Basel, 2013.

45 Stiller, C.-O.; Hjemdahl, P. Lessons from 20 years with COX-2 inhibitors:importance of dose–response considerations and fairplay in comparative trials, J. Intern. Med. 2022, 1–18.

46 Han, M. I.; Küçükgüzel, S. G. Anticancer and Antimicrobial Activities of Naproxen and Naproxen Derivatives, Mini-Rev. Med. Chem. 2020, 20, 1300-1310.

47 Harris, R. E.; Beebe-Donk, J.; Doss, H.; Doss, D. B. Aspirin, ibuprofen, and other non-steroidal anti-inflammatory drugs in cancer prevention: A critical review of non-selective COX-2 blockade, Oncology Reports 2005, 13, 559-583.

48 J. D. Hayes, J. U. Flanagan, I. R. Jowsey, Ann. Rev. Pharmacol. Toxicol. 2005, 45, 51–88.

49 Agonigi, G.; Riedel, T.; Zacchini, S.; Păunescu, E.; Pampaloni, G.; Bartalucci, N.; Dyson, P. J.; Marchetti, F. Synthesis and Antiproliferative Activity of New Ruthenium Complexes with Ethacrynic-Acid-Modified Pyridine and Triphenylphosphine Ligands. Inorg. Chem. 2015, 54, 6504−6512.

50 Neises, B.; Steglich, W. Simple Method for the Esterification of Carboxylic Acids. Angew. Chem., Int. Ed. Engl. 1978, 17, 522 − 524.

51 Dasari, S.; Tchounwou. P. B. Cisplatin in cancer therapy: Molecular mechanisms of action, Eur. J. Pharmacol. 2014, 740, 364–378.

52   Biancalana, L.; Batchelor, L. K.; Funaioli, T.; Zacchini, S.; Bortoluzzi, M.; Pampaloni, G.; Dyson, P. J.; Marchetti, F. α-Diimines as versatile, derivatizable ligands in ruthenium(II) p-cymene anticancer complexes. Inorg. Chem. 2018, 57, 6669 − 6685.

53   Wang, F.; Habtemariam, A.; van der Geer, E. P. L.; Fernández, R.; Melchart, M.; Deeth, R. J.; Aird, R.; Guichard, S.; Fabbiani, F. P. A.; Lozano-Casal, P.; Oswald, I. D. H.; Jodrell, D. I.; Parsons, S.; Sadler, P. J. Controlling ligand substitution reactions of organometallic complexes: tuning cancer cell cytotoxicity, Proc. Natl. Acad. Sci. USA 2005, 102, 18269-18274.

54   Scolaro, C.; Bergamo, A.; Brescacin Delfino, L.; Cocchietto, M.; Laurenczy, G.; Geldbach, T. J.; Sava, G.; Dyson, P. J. In vitro and in vivo evaluation of ruthenium(II)-arene PTA complexes. J. Med. Chem. 2005, 48, 4161-4171.

55   Meier-Menches, S. M.; Gerner, C.; Berger, W.; Hartinger, C. G.; Keppler, B. K. Structure–activity relationships for ruthenium and osmium anticancer agents – towards clinical development, Chem. Soc. Rev. 2018, 47, 909-928.

56    $^{31}P\{^1H\}$ NMR (CDCl$_3$): δ/ppm = 38.3.

57   Experiments were conducted at 37 °C following the procedures reported in the Experimental section for analogous stability studies, by dissolving complexes **4-7** in CD$_3$OD/D$_2$O 1:2 v/v solution (0.75 mL) containing Me$_2$SO$_2$ as standard. The percentage amount of ethacrynic acid generated from **4** in this condition was 47% after 20minutes at room temperature. The percentage of residual complex +related aquo species ranged from 75% to 90% in the cases of **5-7**.

58   Chatterjee, S.; Biondi, I.; Dyson, P. J.; Bhattacharyya, A.; A bifunctional organometallic ruthenium drug with multiple modes of inducing apoptosis. *J. Biol. Inorg. Chem.*, **2011**, *16*, 715-724.

59   Johansson, K.; Ito, M.; Schophuizen, C. M. S.; Thengumtharayil, S. M.; Heuser, V. D.; Zhang, J.; Shimoji, M.; Vahter, M.; Ang, W. H.; Dyson, P. J.; Shibata, A.; Shuto, S.; Ito, Y.; Abe, H.; Morgenstern, R. Characterization of New Potential Anticancer Drugs Designed To Overcome Glutathione Transferase Mediated Resistance. *Mol. Pharmaceutics*, **2011**, *8*, 1698-1708.

60   Cynkowska, G.; Cynkowski, T.; Al-Ghananeem, A. A.; Guo, H.; Ashton, P.; Crooks, P. A. Novel antiglaucoma prodrugs and codrugs of ethacrynic acid. *Bioorg. Med. Chem. Lett.*, **2005**, *15*, 3524–3527.

61 S. A. P. Pereira, F. D. Bobbink, P. J. Dyson, M. L. M. F. S. Saraiva, Automatic evaluation of cyclooxygenase 2 inhibition induced by metal-based anticancer compounds, J. Inorg. Biochem. 2021, 218, 111399.

62 Biancalana L, Batchelor L K, Pereira S A P, Tseng P J, Zacchini S, Pampaloni G, Saraiva L M F S, Dyson P J, Marchetti F. Bis-conjugation of Bioactive Molecules to Cisplatin-like Complexes through (2,2'-Bipyridine)-4,4'-Dicarboxylic Acid with Optimal Cytotoxicity Profile Provided by the Combination Ethacrynic Acid/Flurbiprofen. Chem. Eur. J. 2020, 26, 17525-17535.

63 Reger, D. L. Syntheses of tris(pyrazolyl)methane ligands and {[tris(pyrazolyl)methane]Mn(CO)$_3$}SO$_3$CF$_3$ complexes: comparison of ligand donor properties. J. Organomet. Chem. 2000, 607, 120–128.

64 Menges, F. "Spectragryph - optical spectroscopy software", Version 1.2.5, @ 2016-2017, http://www.effemm2.de/spectragryph.

65 Fulmer, G. R.; Miller, A. J. M.; Sherden, N. H.; Gottlieb, H. E.; Nudelman, A.; Stoltz, B. M.; Bercaw, J. E.; Goldberg, K. I. NMR Chemical Shifts of Trace Impurities: Common Laboratory Solvents, Organics, and Gases in Deuterated Solvents Relevant to the Organometallic Chemist. Organometallics 2010, 29, 2176–2179.

66 Willker, W.; Leibfritz, D.; Kerssebaum, R.; Bermel, W. Gradient selection in inverse heteronuclear correlation spectroscopy. Magn. Reson. Chem. 1993, 31, 287-292.

67 Sheldrick, G. M. Crystal structure refinement with SHELXL. Acta Crystallogr. C2015, 71, 3-8.

68 N. M. Rice, H. M. N. H. Irving, M. A. Leonard, Nomenclature for liquid-liquid distribution (solvent extraction) (IUPAC Recommendations 1993), Pure Appl. Chem. 1993, 65, 2373-2396.

69 a) OECD Guidelines for Testing of Chemicals, in OECD, Paris: 1995; Vol. 107. b) J. C. Dearden, G. M. Bresnen, The Measurement of Partition Coefficients, Quant. Struct.-Act. Relat. 1988, 7, 133-144.

70 D. J. Currie, C. E. Lough, R. F. Silver, H. L. Holmes, partition coefficients of some conjugated heteroenoid compounds and 1,4-naphthoquinones, Can. J. Chem. 1966, 44, 1035-1043.

71 T. Rundlöf, M. Mathiasson, S. Bekiroglu, B. Hakkarainen, T. Bowden, T. Arvidsson, Survey and qualification of internal standards for quantification by 1H NMR spectroscopy, J. Pharm. Biomed. Anal. 2010, 52, 645–651.

72 Calculated by the formula pD = pH* + 0.4, where pH* is the value measured for H$_2$O-calibrated pH-meter. a) C. C. Westcott, pH Measurements; Academic Press: New York, **1978**. b) A. K. Covington, M. Paabo, R. A.

Robinson, R. G. Bates, Use of the glass electrode in deuterium oxide and the relation between the standardized pD (paD) scale and the operational pH in heavy water, *Anal. Chem*. **1968**, *40*, 700-706.

73 T. Mosmann, Rapid colorimetric assay for cellular growth and survival: application to proliferation and cytotoxicity assays, J. Immunol. Methods 1983, 65, 55–63.